J. Fluid Mech. (1983), *vol.* 128, *pp.* 283–322
Printed in Great Britain

On the role of wall-pressure fluctuations in deterministic motions in the turbulent boundary layer

By A. S. W. THOMAS† AND M. K. BULL
Department of Mechanical Engineering, University of Adelaide, South Australia

(Received 17 May 1982)

The wall-pressure fluctuations beneath a turbulent boundary layer have been conditionally sampled on a basis of the high-frequency activity of the pressure fluctuations themselves, the high-frequency activity of the streamwise velocity fluctuations in the vicinity of the wall, and the excursions in velocity in the vicinity of the wall. This has led to the identification of a characteristic wall-pressure fluctuation pattern which is associated with the burst–sweep cycle of events in the wall region. The pattern has the form of an overpressure over a streamwise extent of about $1{\cdot}5$–$2{\cdot}0\delta_*$, with a region of underpressure and a pressure minimum to either side of it, the distance between pressure minima being about $3{\cdot}0$–$3{\cdot}5\delta_*$. This pattern is convected at a velocity 0·67 times the freestream velocity. Its phase relationship with velocity fluctuations close to the wall and the wall shear-stress fluctuations during the burst–sweep cycle have been established. It appears to be produced by the inclined shear layer which forms the upstream surface of the large organized structures in the layer, and calculated pressure patterns support this conclusion.

The phase relationships indicate that fluid involved in the bursting process is subjected to a favourable streamwise pressure gradient by the characteristic wall-pressure pattern at the time that the lift-up of low-speed streaks in the wall region begins. In addition, order-of-magnitude estimates suggest that the adverse pressure gradients associated with the characteristic pressure pattern, even if their phasing with streak lift-up were appropriate, would be insufficient to initiate the lift-up. It is therefore concluded that the streamwise pressure gradients associated with the pressure patterns do not play an active role in the dynamics of the wall flow and are not the direct cause of the bursting process.

1. Introduction

Intensive research by a large number of investigators over the past ten to fifteen years has led to greatly increased knowledge of the structure of the turbulent boundary layer, and of the physical details of the organized fluid motions that are responsible for it. A comprehensive account of the results of this work is given in an excellent review by Willmarth (1975). In this paper we are concerned primarily with the character and role of pressure fluctuations due to the organized structure in the mechanics of the turbulent processes.

In broad terms, two types of organized motion within the boundary layer can be identified: an ordered cyclic sequence of events in the wall region, and a large-scale motion in the outer layer with a scale of the order of the boundary-layer thickness. The former was first revealed by the Stanford flow-visualization work of Kline *et al.*

† Present address: Lockheed-Georgia Company, Marietta, Georgia 30063, U.S.A.

(1967), and then further elucidated by Kim, Kline & Reynolds (1971) and Offen & Kline (1974). It has also been studied independently by Corino & Brodkey (1969) and later Nychas, Hershey & Brodkey (1973), and it is now generally known as the burst–sweep cycle of events. It is characterized by the formation close to the wall of streamwise streaks of low-speed and high-speed fluid, the lift-up of the low-speed streaks from the boundary surface, their subsequent oscillation and disintegration ('break-up') into random small-scale motion, and finally removal of fluid involved in this bursting process by a 'sweep' of high-speed fluid. The other type of organized motion, the large-scale structure, has been studied by Kaplan & Laufer (1969), Kovasznay, Kibens & Blackwelder (1970), Antonia (1972) and others, using correlation and conditional-sampling techniques, and by Falco (1977) using flow-visualization techniques. The first indication of a possible interdependence of these two types of motion was given by Rao, Narasimha & Badri Narayanan (1971), who observed that the mean period of the burst–sweep cycle scales on outer layer variables, that is on the variables that characterize the large-scale organized motion. This was subsequently substantiated by the work of Laufer & Badri Narayanan (1971) and Lu & Willmarth (1973), but has recently been questioned by Blackwelder & Haratonidis (1980). In another aspect of the present investigation reported by Brown & Thomas (1977), however, it has been shown by a more direct approach, based on detailed measurements of velocity and wall shear-stress fluctuations, that recurrent increases in the level of small-scale turbulent activity in the wall region are correlated with the passage of large-scale organized structures in the outer region of the boundary layer. These observations suggest that the flow in the outer part of the layer in some way initiates or controls events that occur in the wall region.

Various models have been proposed to explain the organized motions near the wall and in the outer layer and their interaction. A number of these involve hypotheses concerning the role of fluctuating pressures or more particularly the streamwise pressure gradients in the observed flow processes. For example, Offen & Kline (1974) have suggested a detailed model, based on flow-visualization studies, according to which the cyclic occurrence of bursts is due to the convected vorticity from one burst imposing an adverse pressure gradient on a newly forming low-speed streak further downstream. This promotes the lift-up of the streak by means of what they view as a convected local separation of the wall layer. Further, Offen & Kline attribute the organized large-scale motion in the outer part of the boundary layer to the repeated 'pairing' of vortices, associated with the bursting process, which are convected into this region.

To test Offen & Kline's hypothesis that the bursting process is initiated by the imposition of a temporary adverse pressure gradient on a low-speed streak, Willmarth (1975) carried out conditional-sampling experiments to determine the characteristic wall-pressure pattern that is associated with bursting. The result obtained indicates that before the occurrence of a burst, when the velocity close to the wall is low and decreasing, the fluid that is subsequently involved is subjected to a local adverse pressure gradient. However, from the large scale of the observed wall-pressure pattern, Willmarth concludes that the formation of low-speed streaks in the sublayer and the initiation of the bursting process are both the effects of a gross large-scale motion. The initiation of the vorticity associated with a burst are seen as resulting from the formation of an unstable high-shear layer near the wall which is a consequence of the 'massaging' of low-speed sublayer fluid by adverse wall-pressure gradients associated with the convection to the outer layer of large-scale vorticity from previous bursts. In the model of Offen & Kline the outer region of the boundary

layer does not play a direct part in initiating or maintaining the burst–sweep sequence, whereas in Willmarth's extension of the model this large-scale motion controls the wall-region events; the extended model, in this respect, therefore appears to be more consistent with the observation of Laufer & Badri Narayanan (1971) and other workers, which have been referred to earlier. In Willmarth's model it is the pressure field of the large-scale motion that constitutes the link between motion in the outer part of the layer and that in the wall region.

Similar and more extensive conditional pressure-sampling experiments have been made by Burton (1974). These also lead to the identification of a characteristic pressure pattern associated with the bursting process, which, like Willmarth's, seems to imply that sublayer fluid is subjected to an adverse pressure gradient before bursting commences. However, these patterns are not entirely in agreement with those obtained by Willmarth, a point to which we shall return later, in §§6.5 and 6.6.

Earlier work on wall-pressure fluctuations, in particular on narrowband space–time correlations and both narrowband and broadband convection velocities (Willmarth & Wooldridge 1962; Bull 1967), shows that the pressure 'eddies' that make up the wall field can be divided into two families characterized by different wavenumber ranges: a low-wavenumber family convected at velocities typical of the outer part of the boundary layer, and a high-wavenumber family convected at speeds typical of the wall region. This subdivision is consistent with the two scales of organized motion in the boundary layer which play such an important part in determining its structure. Further, recent work (see e.g. Emmerling 1973) indicates that the small-scale pressure fluctuations were very incompletely measured in earlier investigations; in a detailed interferometric study of instantaneous wall-pressure distributions, Emmerling has shown that intense small-scale wall-pressure fluctuations can be identified, and that their occurrence is periodic with a mean period that is very close to that of the burst–sweep cycle as determined by Rao *et al.* (1971) and Lu & Willmarth (1973).

Considerations such as those that have been briefly outlined clearly indicate a need to understand the role of wall-pressure fluctuations in the deterministic processes that are behind the random turbulent motion in the boundary layer. They provided the motivation for the work which is reported here. In this work, aimed at relating the wall-pressure fluctuations to both wall events and the large-scale structure of the layer, an approach considerably different from those of both Willmarth (1975) and Burton (1976) has been taken. As will be seen, however, in order to interpret the results obtained satisfactorily we were led to additional experiments, including some very similar to those performed by Willmarth and Burton.

2. Experimental apparatus and instrumentation

The wind tunnel used in the investigation is an open-circuit type, flow being induced from the atmosphere. It is driven by a centrifugal compressor located downstream of the working section, and has a sonic throat between the downstream end of the working section and the compressor to prevent upstream propagation of compressor noise. To minimize test-section vibration, the working section and inlet section of the tunnel are elastically suspended from the laboratory ceiling. The working section is 5 m long, 230 mm wide, and nominally 230 mm deep; three sides of it are formed by heavy extruded aluminium sections, while the floor consists of a thin flexible steel sheet which can be adjusted to control the mean pressure gradient in the flow. For the present work the floor was set to give zero pressure gradient.

U_0	36·3 m/s	θ	4·2 mm
U_τ	1·28 m/s	Re_θ	10200
δ	40·3 mm	x	3·5 m
δ_*	5·5 mm		

TABLE 1

Results will be presented only for the flow conditions summarized in table 1. Similar results were obtained for flows with lower Reynolds numbers (down to $Re_\theta = 4920$) and the question of a possible Reynolds-number dependence will be discussed later.

Wall shear-stress fluctuations were measured with small rectangular (0·25 × 0·5 mm) hot films manufactured by the vacuum deposition of nickel onto glass. A shock tube test for these devices showed a step response time of about 50 μs, which was well within the desired range. Calibration was achieved using the rotating-disk apparatus of Brown & Davey (1971) and in all cases the measured wall shear was within 5 % of the value given by Preston-tube measurements. A dynamic calibration was inferred from the steady-state calibration by assuming quasi-steady heat transfer with the appropriate correction to account for the reduced spread of heat flux into the substrate at higher frequencies. For full details the reader is referred to Thomas (1977).

Velocity fluctuations were measured using tungsten wires of 5 μm diameter with their ends copper plated to give an active length of 1 mm. Constant-temperature operation was used.

The wall-pressure fluctuations were measured with small piezoelectric transducers, which have been previously described in detail by Bull & Thomas (1976). Originally, it was intended that pinhole-orifice microphones would be used to achieve a high signal-to-noise ratio. However, some preliminary spectral studies (Bull & Thomas 1976) showed disparities between the results from these devices and those from the piezoelectric transducers (which do not introduce any surface discontinuity). Consequently, all pressure measurements were made with piezoelectric transducers. The sensing area of the transducers was circular with a 0·75 mm diameter, corresponding to $dU_\tau/\nu = 65$ or $d/\delta_* = 0{\cdot}14$. The face of the transducer was covered with a thin coating of epoxy resin, which was dressed off to a flat and continuous surface when mounted in the wind-tunnel instrumentation plug. A FET preamplifier was mounted just behind the transducer for impedance matching. Shock-tube tests of the total system indicated a time response to a pressure step of the order of 2 μs.

All data analysis for this work was performed on a CDC 6400 digital computer, the data being recorded with a small data-acquisition system and written onto computer tape. The analog-to-digital converters operated with an 8 bit precision and each record of data consisted of 2560 data points; 16 such records were used to achieve stationarity of the averages that were computed. A sampling rate of 12·5 kHz was used, which corresponds to a Nyquist folding frequency of 6·25 kHz or, in non-dimensional terms, $\omega\delta_*/U_0 = 6{\cdot}0$ or $\omega\nu/U_\tau^2 = 0{\cdot}36$. Spectral measurements show that all but about 7 % of the mean-square signal energy is associated with frequencies below this so that little frequency folding should occur. Subsequent analysis shows no apparent distortion of results due to this phenomenon.

It should also be noted that the signal-to-noise ratio for the transducers was poor for frequencies less than about 200 Hz and at such frequencies reliable spectral

measurements could not be made. But, despite this no attempt was made to eliminate this low-frequency portion of the signal for the purposes of correlation or conditional sampling measurements.

3. Wall-pressure fluctuations and burst signatures

In incompressible turbulent flow the fluctuating pressure p is related to the fluctuating velocity by the Poisson equation

$$\frac{\partial^2 p}{\partial x_i^2} = -\rho q, \tag{1}$$

where the source term q is given by

$$q = 2\frac{\partial U_i}{\partial x_j}\frac{\partial u_j}{\partial x_i} + \frac{\partial^2}{\partial x_i \partial x_j}(u_i u_j - \overline{u_i u_j}), \tag{2}$$

and U_i and u_i are respectively the mean and fluctuating velocity components in the x_i direction. For a wall-bounded flow, if contributions from surface integrals are neglected, the fluctuating pressure at a point $\mathbf{x}$ on the wall is then given by

$$p_w(\mathbf{x}) = \frac{\rho}{2\pi}\int_{y>0} q(\mathbf{x}_s)\frac{dV(\mathbf{x}_s)}{|\mathbf{x}-\mathbf{x}_s|}, \tag{3}$$

where the volume integration is over the entire half-space containing the flow. This indicates that sources over a region of the flow (in principle a semi-infinite region) will contribute to the pressure fluctuations at a given point, and that the contributions from various source regions will fall off rapidly with their distance from the point under consideration.

Since the motion associated with the burst–sweep sequence originates in the sublayer with break-up occurring in the region $10 < y^+ \leqslant 30$ (Kline *et al.* 1967), such events, which result in the generation of velocity fluctuations, might be expected to contribute significantly to the wall-pressure fluctuations. In particular, one might expect to find periods of increased wall-pressure fluctuations at a given observation point as a result of bursts that occur in its immediate vicinity. This would be consistent with the features of the wall pressure that follow from (3), but on the other hand it would not be too surprising if the existence of such signatures were obscured by the general contribution from all source regions. In fact, examination of time histories of the wall-pressure fluctuations in isolation does not lead to the identification of what could be unambiguously interpreted as burst signatures.

4. Relationship between wall-pressure and wall-shear fluctuations

In contrast to the observation noted in §3, intermittent intense high-frequency activity can be observed in the fluctuating wall shear stress, and it is likely that this can be associated with bursting. It has also been observed (Brown & Thomas 1977) that this shear activity occurs when the slowly varying part of the wall shear is high. The effect becomes more apparent when the shear-stress signal is split into low- and high-frequency parts (by low- and high-pass filtering with the same cutoff frequency in each case), a process which can be regarded as dividing the signal into two parts which represent large-scale and small-scale motions. In the present work this

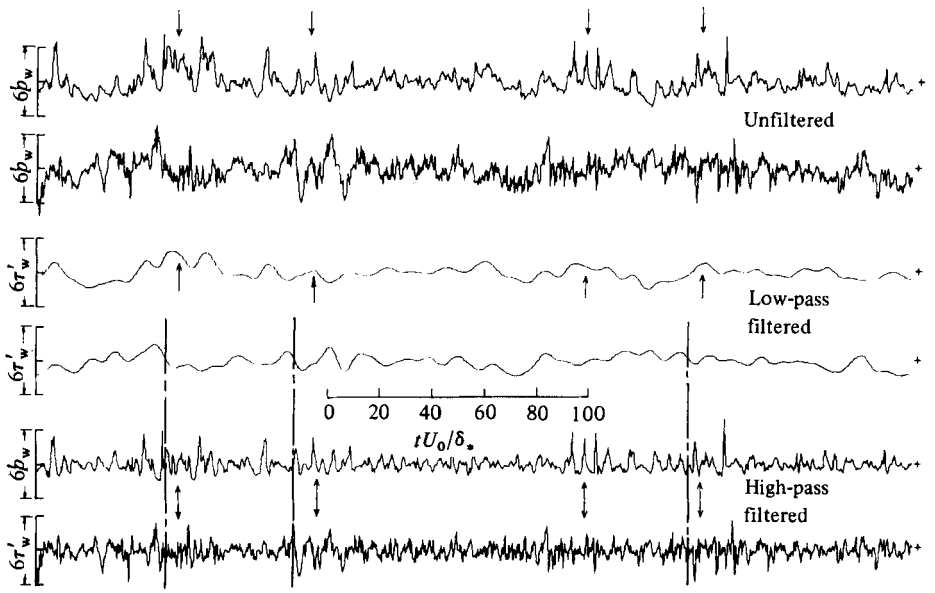

FIGURE 1. Simultaneous time records of the wall shear-stress and the wall-pressure signals. Also shown are the low-pass and high-pass filtered signals. Arrows indicate periods of intense high-frequency wall-shear activity. (Note that the shear signal is taken at a point $1{\cdot}2\delta_* = 540\nu/U_\tau$ downstream of the pressure.) Vertical broken lines indicate correspondence between high-frequency pressure activity and zero-crossings of the low-frequency pressure with negative slope.

technique has been applied to both the wall-pressure and wall-shear signals. (It might be noted here that the notion of investigating the correlation between fluctuations of high frequencies or wavenumbers in a given turbulence signal and the corresponding fluctuations of low frequency or wavenumber was also suggested by Mollo-Christensen (1971).)

The procedure used was in fact to low-pass filter the signals and to obtain the high-pass filtered signal by difference. The filter used was a two-pass zero-phase-delay summing digital filter with a -3 dB cutoff (radian) frequency, based on the outer-layer variables displacement thickness and freestream velocity, of $\omega_c \delta_*/U_0 = 0{\cdot}43$. The cutoff frequency was chosen on the basis of several considerations: to correspond to the frequency range where the spectra of both the fluctuating wall shear stress (Thomas 1977, 1979) and fluctuating pressure (Bull & Thomas 1976) show transition from outer-layer scaling to inner-layer scaling; to include the bursting frequency (assumed to be characteristic of organized large-scale motion) well within the low-pass frequency range (the value chosen being about twice the bursting frequency, as given by $TU_0/\delta_* \approx 30$, determined by Rao *et al.* 1971); and to give what was judged by inspection to be acceptable smoothing of the original signal (see figure 8 of Brown & Thomas 1977). It is also consistent with the dividing frequency between high- and low-wavenumber components of the wall-pressure field given by Bull (1967) as $\omega\delta_*/U_0 \approx 0{\cdot}3$.

Simultaneous records of wall pressure and wall shear, taken with the hot film immediately downstream of and as close as possible to the pressure transducers are shown in figure 1. (The actual separation distance is $\xi/\delta_* = 1{\cdot}2$ or $\xi^+ = 540$; the corresponding convective time delay between the two instruments is therefore $\tau U_0/\delta_* \approx 2$.) The figure also shows the corresponding low- and high-pass filtered signals. The high-frequency shear signal clearly shows periods of intense activity

(marked with arrows in figure 1) interspersed with periods of relative quiescence. Comparison of high-frequency and low-frequency signals shows that at times of intense high-frequency activity the low-frequency, slowly varying, part of the wall shear almost invariably has a high positive value, typically greater than the r.m.s. value τ'_w of the total fluctuating shear.

Since the same flow processes that are responsible for this relationship between the small-scale and large-scale flow components of the wall shear must also be responsible for generating wall-pressure fluctuations, some similar relationship might be expected between the corresponding components of the wall pressure. Inspection of the wall-pressure signals, without reference to the shear signals, indicates that there are periods of more-intense activity, but in general they do not stand out in the high-frequency signal nearly as obviously as in the case of the shear fluctuations; there is furthermore no obvious correlation between these more-intense high-frequency pressure fluctuations and the corresponding low-frequency variations. However, examination of the high-frequency pressure signals for intense activity, with the times of occurrence of intense high-frequency shear activity as a guide, shows that on some occasions the two do appear to occur at about the same time, indicating that small-scale wall-pressure fluctuations, as well as small-scale wall-shear fluctuations, are, to some extent, correlated with the large-scale flow component of the wall shear. The correlation for the pressure is clearly not as strong as that for the shear, but, given its existence, this might be expected, since any such correlated pressure fluctuations will occur together with contributions from other pressure sources in the general vicinity of the point, in accordance with (3).

5. Correlation between small-scale and large-scale wall-pressure fluctuations

The correlation between the high- and low-frequency components of a given signal has been so far considered in terms of the relation of finite periods of high-frequency activity with increased amplitude to the corresponding low-frequency variations. To quantify this relationship a direct calculation of the correlation between the two signal components would clearly be inappropriate, but correlation between the low-frequency signal and the amplitude of the envelope of the high-frequency signal would seem to provide the type of measure required. In fact, it was found more convenient to achieve essentially the same result by using the rectified high-frequency signal, adjusted to have zero mean value, and then smoothed by low-pass filtering using the same non-dimensional filter cutoff frequency as previously ($\omega_c \delta_*/U_0 = 0{\cdot}43$). Results of applying this technique to the wall-shear signals have been reported by Brown & Thomas (1977). Typical results, for three different filter settings, are reproduced in figure 2. The high positive value of the maximum correlation clearly confirms the previous conclusion based on inspection of time histories such as those in figure 1. (It should be noted that similar tests were performed with white noise and with appropriately skewed synthetic random signals. These confirmed that the correlation does not result from the character of the procedure itself.) The same technique has been applied to the wall pressure signals, with the result shown in figure 3. The correlation coefficient in this case is

$$R = \frac{1}{p'_{\mathrm{hrs}}\, p'_{\ell}} \lim_{T \to \infty} \int_0^T p_{\mathrm{hrs}}(t)\, p_{\ell}(t+\tau)\, dt,$$

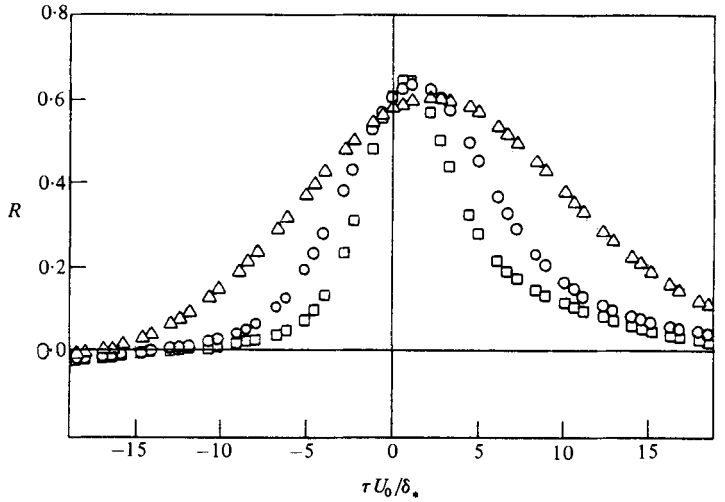

FIGURE 2. Correlation between the low-frequency component and the smoothed rectified high-frequency component of the wall shear, for various filter cutoff frequencies. △, $\omega_c \delta_*/U_0 = 0{\cdot}9$; ○, 0·43; □, 0·21.

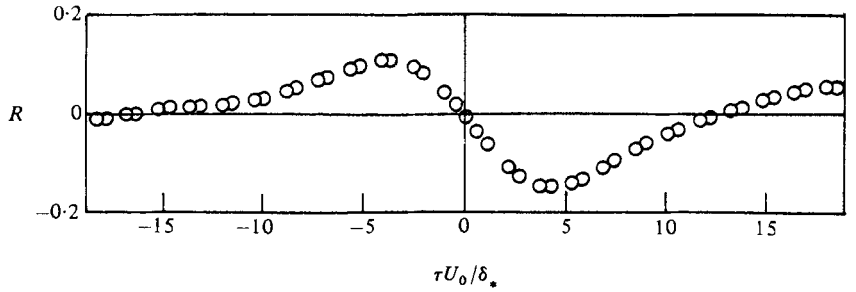

FIGURE 3. Correlation between the low-frequency component and the smoothed rectified high-frequency component of the wall pressure; $\omega_c \delta_*/U_0 = 0{\cdot}43$.

where p_{hrs} and p_ℓ are respectively the smoothed rectified high-frequency and low-frequency signals, and the primes signify r.m.s. values (also based on long time averages). Figure 3 shows that the low- and high-frequency components of the wall pressure are interdependent. The low maximum values of the correlation coefficient are consistent with the earlier discussion, in §4, of the characteristics of the pressure signals that can be seen by inspection of the time histories.

One possible interpretation of figure 3 is that large high-frequency pressure fluctuations occur most frequently when the slowly varying part of the pressure is falling from a large positive value, through zero, to a large negative value. Examination of records such as those in figure 1 reveals that there are occasions when such behaviour can be observed; some can be seen in figure 1, and in these cases the correspondence between a zero-crossing of the low-frequency pressure signal with negative slope and large-amplitude high-frequency pressure fluctuations has been marked. It is clear from figure 1 and from other records examined that by no means do all such zero-crossings of the low-frequency pressure signal coincide with increased high-frequency activity. It appears that the two do generally occur simultaneously at times coinciding fairly closely with increased high-frequency shear activity (which can be seen from figure 1 when allowance is made for the small convective time delay

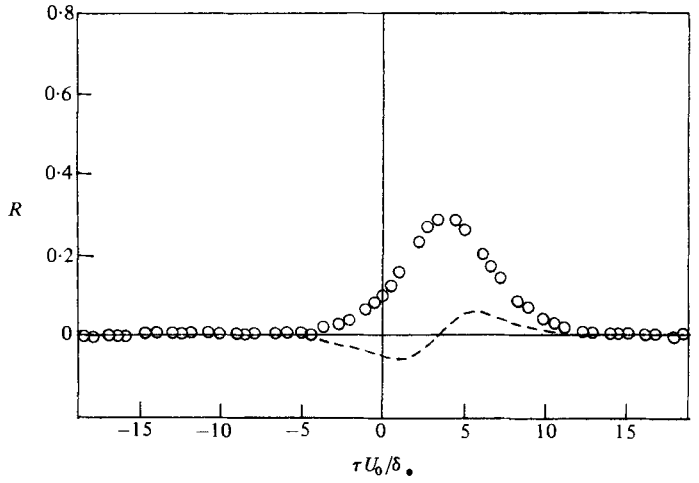

FIGURE 4. Correlation between the smoothed rectified high-frequency wall shear and the smoothed rectified high-frequency wall pressure; $\omega_c \delta_*/U_0 = 0{\cdot}43$. The dashed line corresponds to the broadband correlation between the two signals.

of $\tau U_0/\delta_* \approx 2$ between pressure and shear signals), although they also occur simultaneously at other times, when the high-frequency shear signal is quiescent.

Some direct measurements of the correlation between wall-pressure and wall-shear fluctuations have also been made. Correlation between the broadband signals gives a correlation curve as a function of time delay of the same forms as those of pressure and streamwise velocity fluctuations obtained by Willmarth & Wooldridge (1963). As shown in figure 4 the curve has a zero-crossing at a time delay corresponding to the time of convection between the two measuring points. In contrast, correlation between the smoothed rectified high-frequency pressure signal and the smoothed rectified high-frequency shear-stress signal gives positive correlation values over a wide range of time delays, with a maximum correlation coefficient of 0·3 at virtually the same time delay as that at which the broadband correlation has its zero-crossing (see figure 4). This reinforces the conclusion reached previously (§4) that intense high-frequency pressure fluctuations occur at or about the same time as high-frequency shear-stress fluctuations.

6. Conditional sampling experiments

6.1. *General considerations*

An alternative and more-definite way of establishing whether or not a characteristic low-frequency pressure variation is generally associated with large-amplitude high-frequency pressure fluctuations is by conditional sampling of the pressure signal.

This procedure is based upon the identification of the relationship between a repeated event or salient feature in one random signal and a repeated characteristic variation or pattern in the same or another signal. The characterization of these individual patterns is achieved by sampling the time history over the duration of the pattern, whenever one occurs, and averaging over the ensemble of samples. This requires that all the samples be synchronized on some feature common to all patterns; the resulting average can then be regarded as a typical time history of all such patterns. Also, sampling must be conditioned by the detection of either a salient

feature in the signal containing the patterns (which may be a feature of the patterns themselves) or a salient feature in another signal.

The procedure may seem straightforward enough, but there are a number of factors which should be taken into account in deciding on the details of the procedure to be followed and in interpreting the results that are obtained.

(i) Detection usually involves, as one criterion, determination of the time at which the conditioning signal exceeds or falls below some discriminator level. The appropriate level is not known in advance.

(ii) If the signal to be sampled is also the conditioning signal, care must be taken to ensure that the ensemble average of the samples is not merely a reflection of the detection criterion that is used.

(iii) The success of the procedure in producing samples that are always realizations of the pattern of interest will depend critically on the uniqueness of the salient feature on which detection is based. It is inevitable that, in the random signals typical of turbulent flows, variations resembling the salient feature but unconnected with the patterns will sometimes occur, and that sometimes other contributions to the signal will distort the salient feature to the point where it is no longer recognizable. Such occurrences will lead to the inclusion of samples that should have been omitted and vice versa (although the former is potentially of greater consequence than the latter).

(iv) The detection scheme must lead to the identification of corresponding times in successive patterns to allow synchronization of the time-history samples. Otherwise, the ensemble average of samples, centred on what are assumed to be corresponding times, will be a distorted representation of an average pattern. This again depends on the uniqueness of the salient feature on which detection is based.

(v) Although the patterns may be recognizably similar, there will inevitably be random differences in their timescales and amplitudes. Hence, even if the samples are correctly synchronized, these random differences can lead to ensemble averages unrepresentative of the patterns at times remote from the synchronization time. In the extreme the ensemble average may only represent the true average pattern at times in a very narrow range centred on the synchronization time. (In principle this problem could be overcome by referring each sample pattern to a non-dimensional timescale based on its own time of duration. But, in general, this merely shifts the problem to one of defining the beginning and end of a pattern.)

(vi) Since the success of conditional sampling depends on the uniqueness of the salient feature of the conditioning signal, detection based on a single criterion, such as the magnitude of the excursions of a particular flow variable, will rarely be adequate. Almost invariably greater precision in the definition of the salient feature is required; this may be achieved by taking into account the timescale of the salient feature as well as its amplitude and possibly additional characteristics of the conditioning signal.

Some of these difficulties, and procedures by which that can be alleviated, are discussed by Blackwelder (1977) and by Thomas (1979) (in particular, the technique for enhancement of ensemble averages).

6.2. *Pressure sampling, self-conditioned on small-scale pressure fluctuations*

We now return attention to the establishment of whether or not there is some definite relationship between the low-frequency and high-frequency components of the wall-pressure fluctuations. For this purpose the smoothed rectified high-frequency signal has been used as the conditioning signal; it provides a measure of the amplitude of the high-frequency fluctuations, and, since it is a rectified signal, bias towards

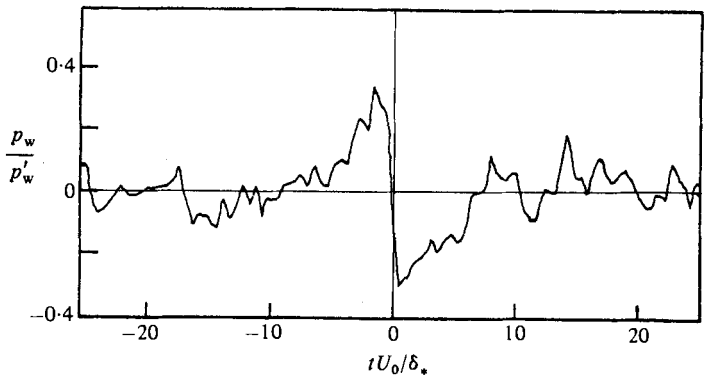

FIGURE 5. Ensemble-averaged time history of conditionally sampled wall pressure. Detection is based on the smoothed rectified high-frequency component of the pressure.

high-frequency fluctuations of any one sign is avoided. Samples of the time history of the pressure fluctuations have been taken, centred on times at which the smoothed rectified high-frequency signal has a local maximum value greater than 1·5 times its r.m.s. level. The use of this criterion follows from Thomas (1977, 1979). The ensemble average of the samples is shown in figure 5.

The form of the resultant ensemble-averaged pattern appears to imply that during periods of high-amplitude high-frequency fluctuation there is a preferred variation of the low-frequency component of the pressure: it rises slowly to a large positive value, falls rapidly through zero to a large negative value, and subsequently returns slowly to a small value. This is exactly the behaviour that was suggested in §5 as a possible explantion of the observed correlation between the low- and high-frequency components of the pressure signal (figure 3). We note that similar pressure patterns – large overpressure followed (in time) by a rapid fall to a large underpressure – have been observed in an optical study of wall-pressure fluctuations by Dinkelacker *et al.* (1977). However, we shall not pursue this comparison any further at this stage, as we shall see later that a rather more detailed consideration must be made of the result that has just been presented.

6.3. *Convection velocity and spatial scale of pressure patterns from self-conditioned sampling*

Convection of pressure patterns and their development during the course of convection can be investigated by means of simultaneously recorded signals, from two wall-pressure transducers, separated by a distance ξ in the streamwise direction, which are then simultaneously conditionally sampled, and the samples ensemble-averaged.

In the case of pressure patterns associated with large-amplitude high-frequency pressure fluctuations, this is achieved by sampling the downstream signal at times determined by the same criterion used to obtain the single-point ensemble average shown in figure 5 (that is, times at which the smoothed rectified high-frequency signal from the upstream transducer has a local maximum greater than 1·5 times its r.m.s. value). Typical ensemble-averaged patterns for several separation distances are shown in figure 6. In each case the pattern at the downstream station has a similar character to that at the upstream station, except for a time delay which increases as the distance between the points increases. As the separation distance increases, the definition of the pattern progressively deteriorates, but it is only at separations exceeding about $15\delta_*$ ($\approx 2\delta$) that it can no longer be clearly identified. This could

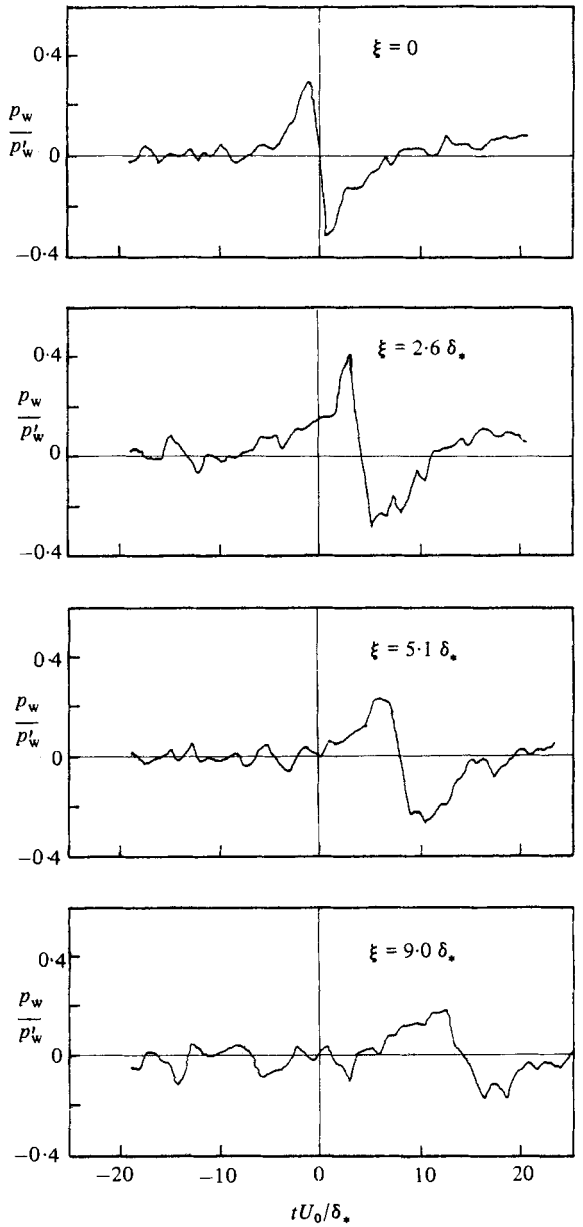

FIGURE 6. Ensemble-averaged time histories of the conditionally sampled wall pressure, for various streamwise distances between the detection and sampling points.

result from loss of coherence of the pattern during convection, but it is to be expected that statistical variations in the patterns themselves and in their convection velocities would also contribute to this effect. It is therefore likely that the patterns retain their identities over even longer times and convection distances than figure 6 indicates.

The most readily identifiable timing feature of the pressure patterns is their zero-crossings, and these have been used to determine convection velocities. Results for three Reynolds numbers, which cover the maximum possible range of the timescale δ_*/U_0 achievable with the present experimental arrangement, are shown

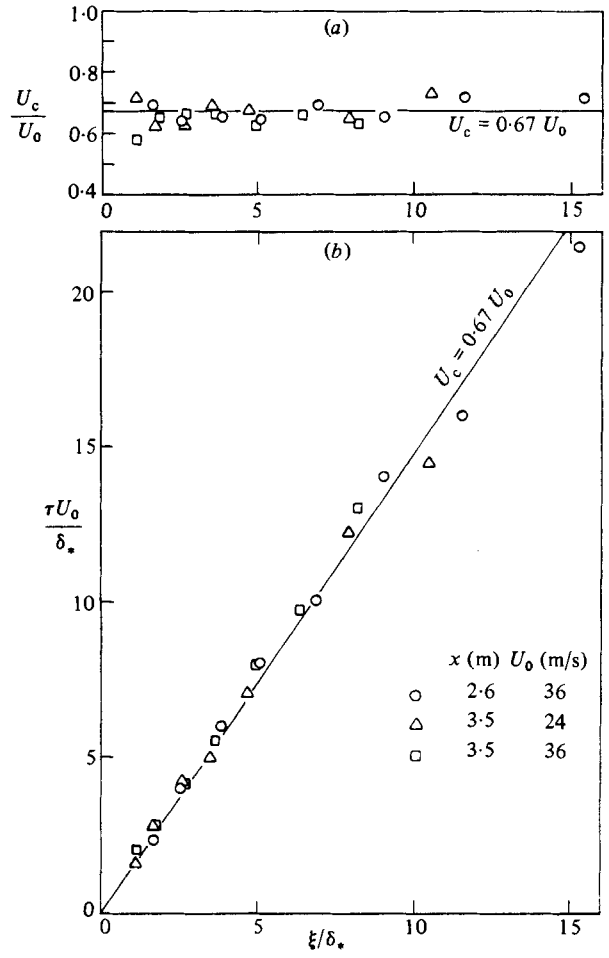

FIGURE 7. (*a*) Convection velocities determined from ensemble-averaged time histories of conditionally sampled wall pressure. (*b*) Variation of time delay with separation distance of pressure transducers.

in figure 7. In all cases the convection velocity appears to be essentially independent of separation distance and has a value of about 0·67 times the freestream velocity.

If, following Willmarth & Wooldridge (1962) and Bull (1967), it is assumed that the sources of the wall-pressure fluctuations are velocity fluctuations convected at local mean-flow velocities, then the sources of the pressure patterns would be located at a distance from the wall of $y/\delta_* \approx 0{\cdot}53$ or $y^+ \approx 250$. From figure 5 the timescale of the patterns is about $tU_0/\delta_* = 15$; with the measured convection velocity, $U_c/U_0 = 0{\cdot}67$, this implies a streamwise lengthscale of about $10\delta_*$, that is, of the order of the boundary-layer thickness. The lateral scale appears to be somewhat smaller than this: the large-amplitude high-frequency wall-pressure fluctuations with which the patterns are associated are observed to occur simultaneouly at points laterally separated by distances of the order of $1{\cdot}5\delta_*$ or $700\nu/U_\tau$; and, consistently with this, the smoothed rectified high-frequency pressure signals are found to be positively (although weakly) correlated over similar lateral distances. These pressure patterns therefore appear to be characteristic of the large-scale motion in the flow rather than the much-smaller-scale wall events.

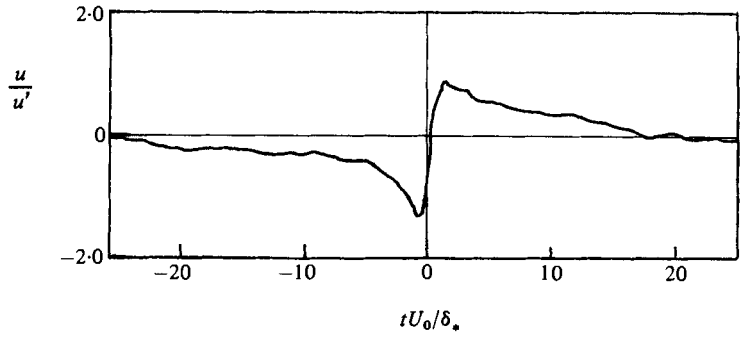

FIGURE 8. Ensemble-averaged time history of conditionally sampled velocity at $y^+ = 30$. Detection is based on the smoothed rectified high-frequency component of velocity.

6.4. *Pressure sampling conditioned on small-scale velocity fluctuations at* $y^+ = 30$

To determine whether the pressure patterns associated with large-amplitude high-frequency pressure fluctuations are also associated with a specific pattern of velocity fluctuations, and in particular those that are known to accompany the bursting process, the pressure signals were also conditionally sampled on the basis of small-scale velocity fluctuations at a point at $y^+ = 30$ directly above the pressure transducer (in reality very slightly downstream of the pressure transducer by a distance $\Delta x^+ = 60$ in order to avoid interference). The pressure signal was sampled whenever the smoothed rectified high-pass-filtered velocity signal (obtained with the same filter cutoff frequency as in the case of the pressure signals, $\omega_c \delta_*/U_0 = 0{\cdot}43$) reached a local maximum value greater than 1·5 times its r.m.s. value.

It might be noted that conditional sampling of the velocity signal itself at $y^+ = 30$ in this way yields an ensemble-averaged velocity pattern of the form shown in figure 8. The pattern is characterized by a sudden sharp step-like rise in velocity. Similar velocity patterns, frequently referred to as burst signatures, at y^+ values of from 5 to more than 40 have been obtained by Blackwelder & Kaplan (1976) using conditional sampling based on the velocity at $y^+ = 15$ (see also Blackwelder 1977). Thomas (1977) has found evidence of these signatures even in the outer part of the layer, and it therefore seems more appropriate to refer to them as characteristics of the large-scale structure with which bursts are strongly associated.

The ensemble-averaged pressure pattern obtained with this velocity criterion is shown in figure 9. It is similar in form to the pattern obtained by using the pressure itself as the conditioning signal (figure 5), with a sharp drop in pressure as its prominent feature, although the timescale is rather shorter (tU_0/δ_* about 10 or less, compared with about 15 previously) and the amplitude of the pressure drop is somewhat smaller. (The reverse procedure – conditionally sampling the velocity at $y^+ = 30$ on the basis of large amplitude of the smoothed rectified high-frequency wall-pressure signal – has also been carried out; it yields an ensemble-averaged velocity pattern similar to that of figure 8.)

Some of the pressure and velocity time records obtained during this experiment are shown in figure 10. Arrows indicate times when the velocity signal satisfies the detection criterion. It can be seen that quite frequently the behaviour of the velocity signal in the vicinity of these times is similar to that of the ensemble-averaged velocity pattern shown in figure 8. On the other hand there is little indication of any preferred pattern in the behaviour of the pressure signal at corresponding times. Pressure patterns of the form indicated by figure 9 are presumably obscured by simultaneous

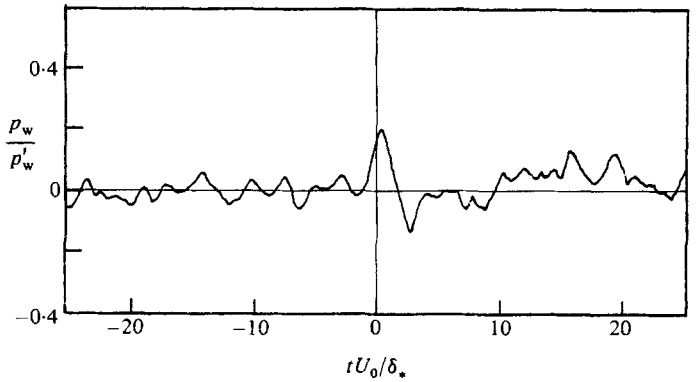

FIGURE 9. Ensemble-averaged time history of conditionally sampled wall pressure. Detection is based on the smoothed rectified high-frequency component of velocity at $y^+ = 30$.

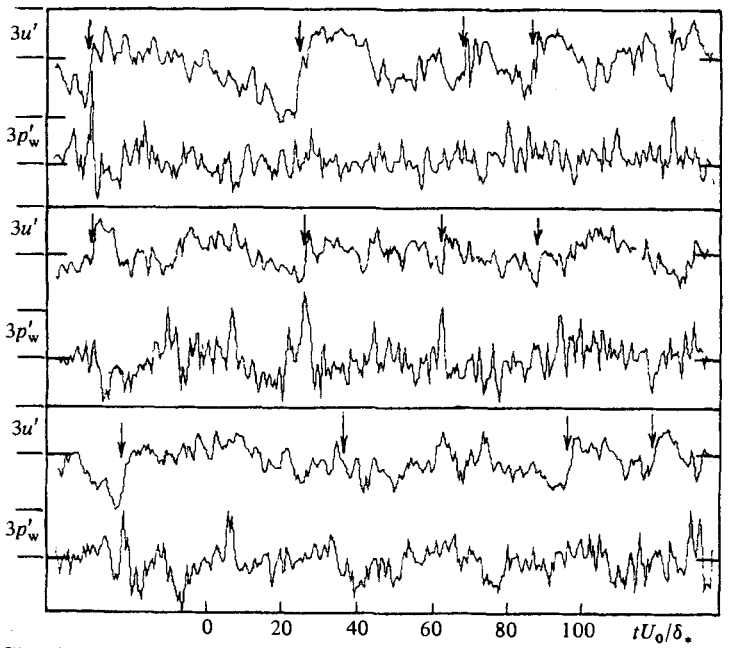

FIGURE 10. Simultaneous time records of the velocity at $y^+ = 30$ and the wall pressure. Arrows indicate the times at which the smoothed rectified high-frequency components of the velocity (not shown) satisfies the detection criterion. (Note that the velocity is measured at a point $60\nu/U_\tau$ downstream of the pressure.)

pressure fluctuations which are uncorrelated with them and which make no contribution to the ensemble average. Such pressure fluctuations would arise from velocity fluctuations in the vicinity of the pressure measuring point, which are uncorrelated with the velocity fluctuations at the point at which the conditioning signal is taken. Despite this, there seems little doubt, from the results presented in this section, that both the large-amplitude high-frequency pressure fluctuations selected by the procedures used in the present work and the large-scale pressure pattern associated with them are intimately connected with the velocity fluctuations near the wall, which are themselves intimately associated with the bursting process.

6.5. *Pressure sampling, conditioned on both u and $\partial u/\partial t$ at $y^+ = 30$*

The characteristic pressure patterns obtained in the present work by correlation of the high- and low-frequency components of the wall-pressure fluctuations and by conditional sampling appear to be self-consistent. However, they are apparently not consistent with previously reported conditional measurements of the wall pressure made by Willmarth (1975) and Burton (1976), and, as noted earlier, the two latter sets of results are apparently not themselves consistent. In the experiments of both Willmarth and Burton the condition for sampling the wall pressure was that the low-pass filtered fluctuating velocity signal at $y^+ = 15$ should be equal to $-2u'$ (where u' is the r.m.s. fluctuation) and decreasing. This criterion was chosen for detection of the outward migration of decelerated fluid which is a characteristic feature of the burst sequence of events. Their results are reproduced in figures 11 (*a*, *b*); they have the common feature that the pressure is at a minimum at the time of detection, but otherwise do not show great similarity. The patterns obtained in the present work (figures 5 and 9), which have been presented in §§6.2 and 6.4, more closely resemble Burton's result (figure 11*b*) in general shape, amplitude and timescale; however, all three patterns appear to be phased differently with respect to the detection time, owing, no doubt, at least in part, to different detection criteria. The pattern obtained by Willmarth (figure 11*a*) has a much larger timescale and a much larger negative peak value.

The physical size of the hot-wire probes in relation to ν/U_τ with the present experimental arrangement precluded the possibility of repeating Willmarth's and Burton's experiments with $y^+ = 15$. But similar experiments were done with the hot wire located at $y^+ = 30$. In one case the cutoff frequency of the low-pass filter used to generate the conditioning signal was $\omega_c \delta_*/U_0 = 1{\cdot}26$, as in Willmarth's experiment, and in the other the unfiltered velocity signal was used as the conditioning signal. (Burton's cutoff frequency, $\omega_c \delta_*/U_0 = 10{\cdot}6$, could not be used since it corresponds to a frequency higher than the Nyquist frequency in the present work.) The results are shown in figures 11 (*c*, *d*). The patterns obtained are very similar to each other, indicating that the result is insensitive to the filtering of the velocity signal, but very different from the Willmarth and Burton results and also from the patterns previously obtained in the present work (figures 5 and 9). Their most-dominant feature is now a steep *rise* in pressure. Even though the detection scheme leading to the patterns shown in figure 11 (*c*, *d*) is intentionally biased towards negative velocity fluctuations, while that leading to figure 9 is unbiased, the dissimilarities among the patterns of figure 9 and figures 11 (*a*–*d*) demanded further investigation.

The wall-pressure signal has therefore been sampled on the basis of the (unfiltered) velocity signal at $y^+ = 30$ for each of the following detection criteria:

(i) $u > u'$ and local maximum ($\partial u/\partial t = 0$);
(ii) $u = u'$ and increasing ($\partial u/\partial t > 0$);
(iii) $u < -u'$ and local minimum ($\partial u/\partial t = 0$);
(iv) $u = -u'$ and decreasing ($\partial u/\partial t < 0$).

A lower discrimination level has been used here in an attempt to reduce statistical uncertainty. The resulting ensemble averages, shown in figure 12, clearly differ according to the sign of the velocity: positive velocities give positive pressures and vice versa. This could imply that the different criteria are identifying totally different flow phenomena, characterized by quite different pressure patterns; or, since all four detection criteria are likely to be satisfied at successive times by a velocity variation of the type represented by figure 8, it could imply that the ensemble averages in figures

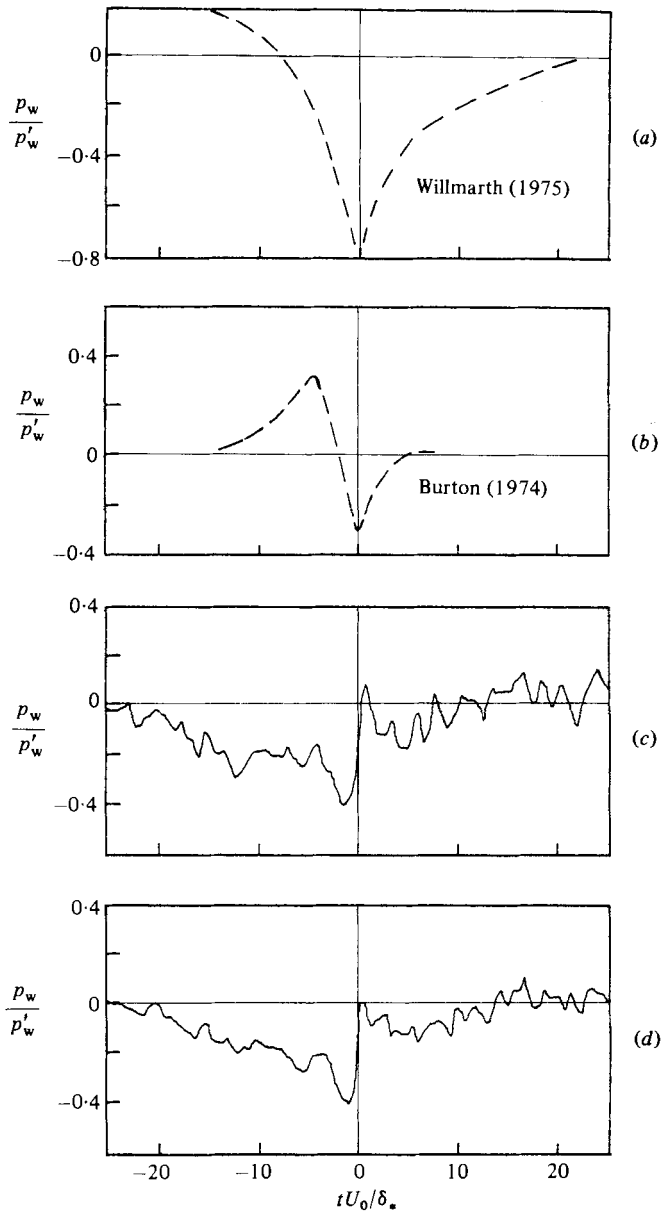

FIGURE 11. Ensemble-averaged time histories of conditionally sampled wall pressure. Detection is based on the low-pass-filtered velocity signal (cutoff ω_c) being equal to $-2u'$ and decreasing (i.e. $\partial u/\partial t < 0$). (*a*) Willmarth (1975); $\omega_c \delta_*/U_0 = 1{\cdot}26$, $y^+ = 15$. (*b*) Burton (1974); $\omega_c \delta_*/U_0 = 10{\cdot}6$, $y^+ = 15$. (*c*) Present tests; $\omega_c \delta_*/U_0 = 1{\cdot}26$, $y^+ = 30$. (*d*) Present tests; velocity signal unfiltered, $y^+ = 30$.

12 (*a–d*) represent different portions of the same pressure pattern, distorted by effects such as those discussed in §6.1.

To test the latter possibility, a search has been made of the velocity signal over a time range, $-10 \leqslant \Delta t U_0/\delta_* \leqslant 10$, centred on each of the high-frequency detection times which lead to pressure patterns such as figure 9, for the nearest times at which the criteria (i)–(iv) of this section are satisfied. For all four criteria, the average difference between the two detection times is found to be small ($|t|U_0/\delta_* \lesssim 2$),

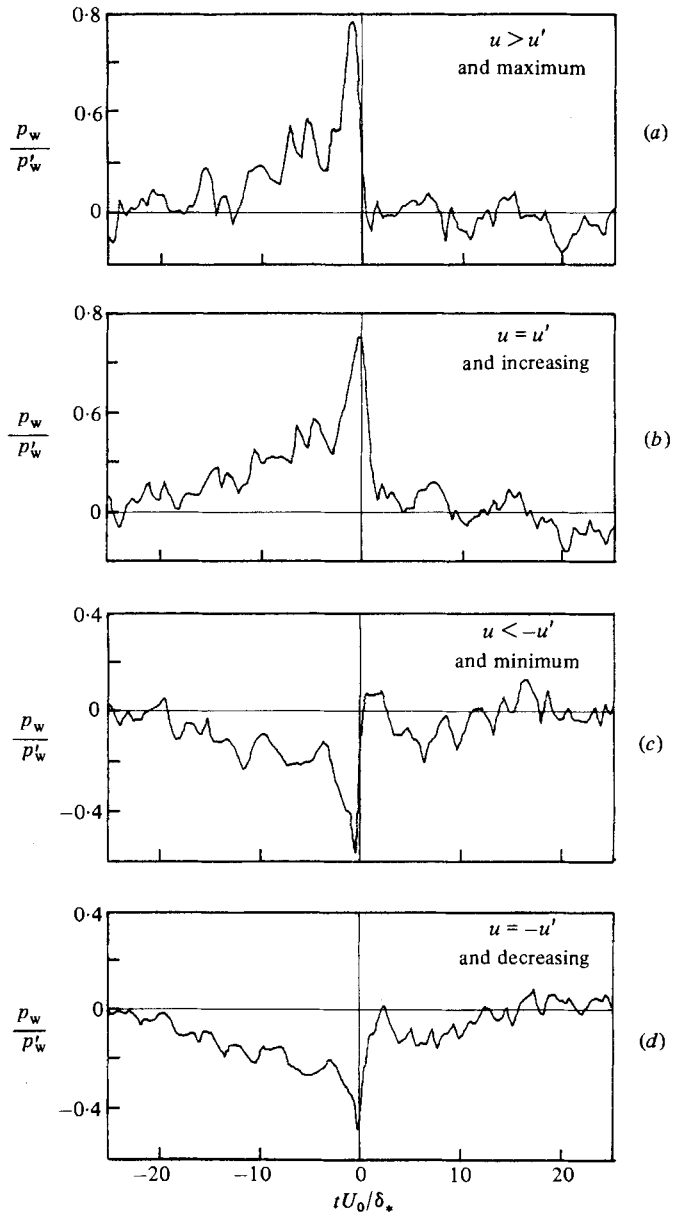

FIGURE 12. Ensemble-averaged time histories of conditionally sampled wall pressure. Detection criteria are indicated on the figures.

suggesting that the various detection criteria all lead to selection of the same pressure pattern but at slightly different times. In this way we obtain new ensembles of pressure patterns, based on detection times determined by the criterion that the velocity signal at $y^+ = 30$ should satisfy one of the conditions (i)–(iv), and that in addition the amplitude of the smoothed rectified high-frequency part of the velocity signal should be greater than $1{\cdot}5u'$ at, or very nearly at, the same time. The ensemble averages are shown in figure 13. Despite the more rigorous detection procedure compared with that leading to figure 12, the four ensemble averages of samples of what must now be the same pressure pattern are still quite different from each other

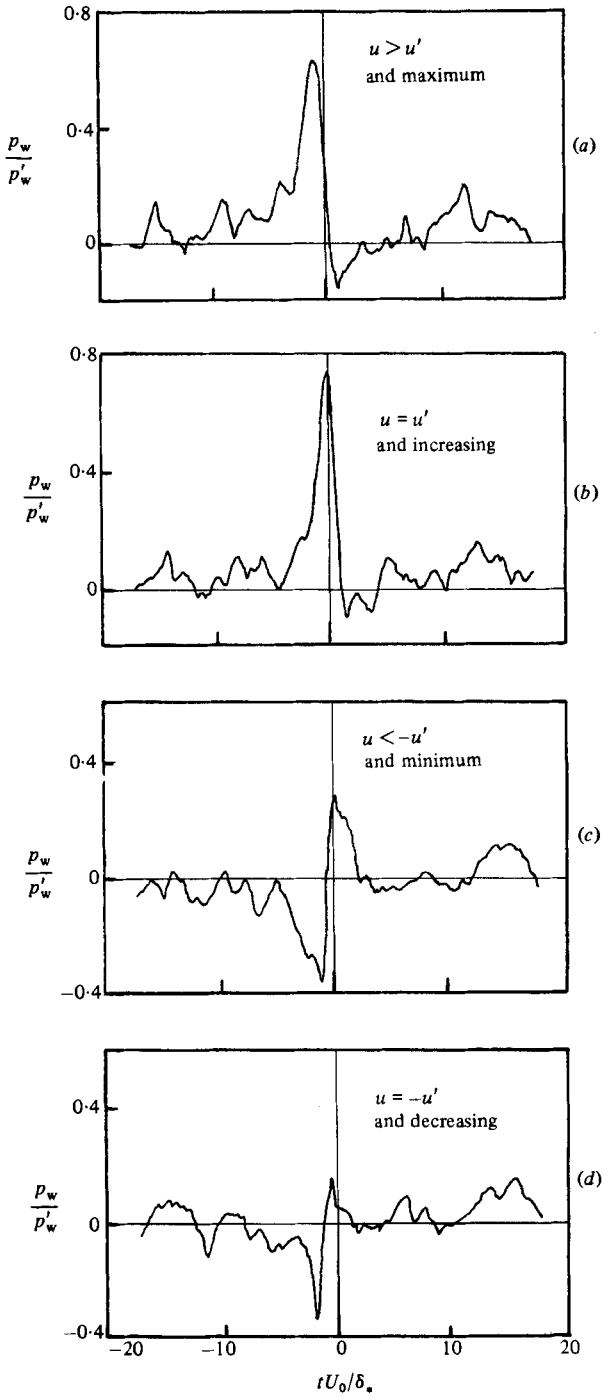

FIGURE 13. Ensemble-averaged time histories of conditionally sampled wall pressure. Detection based on smoothed rectified high-frequency component of wall pressure in addition to the criteria indicated on the figures.

and still similar to the corresponding averages of figure 12. It now seems quite certain that the observed behaviour is due to the different synchronization times combined with statistical variations in pattern amplitudes and timescales; thus the results give a true average of the pressure pattern only at times very close to the synchronization time, and a zero average at times removed from it.

Finally, in this section we note two things. The first is that in no case of conditional sampling based on $u < 0$ and $\partial u/\partial t$ have we obtained an ensemble-averaged pressure pattern that has any extended region of positive pressure at times prior to the detection time, as do Burton's and our own based on smoothed rectified high-frequency signals (§§ 6.2 and 6.4). The second is that the ensemble averages in figures 11 (*c*, *d*) and 12 show, in addition to fairly sharp variations at times near the detection time, a general variation with a larger timescale, $tU_0/\delta_* \approx 30$ or 40. This timescale is comparable to that of the pattern obtained by Willmarth (figure 11*a*); in fact, allowing for amplitude differences, there is some resemblance between figures 11 (*a*) and 12 (*d*). It is much less evident in the ensemble-averaged pressure pattern obtained from sampling conditioned only on the smoothed rectified high-frequency component of the velocity fluctuations at $y^+ = 30$ (figure 9); and it becomes much less noticeable when the u and $\partial u/\partial t$ conditions are supplemented by a condition on the smoothed rectified velocity signal (compare figures 12 and 13). The reason for this behaviour is not clear.

6.6. *Large-scale pressure pattern associated with organized motion at* $y^+ = 30$

On the basis of the results presented in §6.5 we suggest that the true wall-pressure pattern associated with high-amplitude high-frequency velocity activity at $y^+ = 30$, and therefore simultaneously associated with the velocity step at $y^+ = 30$ (as represented by figure 3) and with the bursting process, has a form similar to that shown in figure 14, with the pressure amplitude varying as the velocity gradient. For the moment we shall consider that the phasing of the velocity and pressure variations is as shown in the figure, with the time of occurrence of the pressure peak at the wall coinciding with that of the maximum velocity gradient. In this case, bearing in mind the effects of imperfect synchronization and statistical variations in patterns, it is clear that sampling and averaging the pressure at the times marked in figure 14 as *A*, *B*, *C* and *D* (which correspond to the criteria (*a*), (*b*), (*c*) and (*d*) of figures 12 and 13) would produce pressure patterns like those of figures 12 and 13. Similarly, because of the phasing of the velocity step and the smoothed rectified high-frequency velocity signal (figure 8), detection based only on the latter would be expected to reproduce the dominant central (positive) portion of the suggested pressure pattern, with the peak occurring at the detection time ($t = 0$). The pattern obtained (figure 9) is essentially consistent with this, although the peak does not occur exactly at $t = 0$ but at a slightly later time. Unlike figure 14, the measured pattern is not symmetrical about the central positive peak, although it does show a negative loop at $t > 0$ and a suggestion of a negative loop at $t < 0$. (The corresponding result for a lower flow Reynolds number, not reproduced here, shows similar asymmetry but quite definite negative loops at both $t > 0$ and $t < 0$).

It is now possible to show in a semiquantitative manner how this kind of pressure distribution can arise. First, we note that the step in the streamwise velocity component at $y^+ = 30$, as represented by figure 8, is accompanied by a corresponding sharp drop in the velocity component v normal to the wall. Sampling of both the streamwise and normal fluctuating velocity components (u, v) at different points in the layer at those times at which the streamwise component satisfies the high-

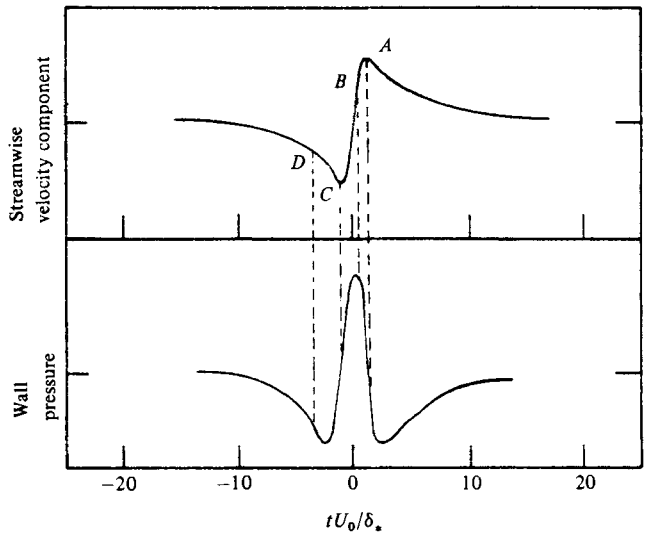

FIGURE 14. Typical streamwise velocity step at $y^+ = 30$ and suggested corresponding wall-pressure pattern.

frequency detection criterion, leads to the set of ensemble averages shown in figure 15. The u-velocity pattern at $y/\delta_* = 0{\cdot}37$ or $y^+ = 170$ is of the same form as for $y^+ = 30$ (figure 8), and, although measurements of v have not been made at $y^+ = 30$, the trends in these data and the data of Blackwelder & Kaplan (1976) suggest that the pattern of v at $y^+ = 30$ will be similar to the pattern of the v-component at $y^+ = 170$ shown in figure 15. We shall now show that a variation of the normal component of the velocity of this form may be expected to give rise to a wall pressure variation like that proposed in figure 14.

The wall pressure fluctuations must satisfy (3), and work by a number of investigators, including Kraichnan (1956), Lilley & Hodgson (1960), Willmarth & Wooldridge (1962), Bull & Lim (1968) and Lim (1971), indicates that, except perhaps at very high frequencies, the dominant contribution to the mean-square pressure comes from the source term associated with turbulence/mean-shear interaction, namely $2(\partial U/\partial y)\,\partial v/\partial x$. If it is assumed that this source term also dominates the instantaneous pressure fluctuations (and this, of course, does not necessarily follow from the evidence for time-averaged quantities), then (3) becomes

$$p_{\mathrm{w}}(\mathbf{x}) = \frac{\rho}{\pi}\int_{y>0} \frac{\partial U}{\partial y}\frac{\partial v}{\partial x}\frac{dV}{|\mathbf{x}-\mathbf{x}_{\mathrm{s}}|}. \tag{4}$$

If it is further assumed that an ensemble-averaged pattern of time variation of the v-component of velocity such as that in figure 15 results from convection of a 'frozen' velocity field, then the pattern can be used to evaluate $\partial v/\partial x$. Then, with $\partial U/\partial y$ known, the corresponding ensemble-averaged pressure variation at the wall can be calculated. Since, on this basis, $\partial/\partial x = -U_{\mathrm{c}}\partial/\partial t$ it is clear that a velocity pattern such as that shown in the lower portion of figure 15 will produce a wall-pressure variation directly under it, of the form postulated in figure 14. The result of such a calculation is shown in figure 16. For the purposes of the calculation it has been assumed that at a given streamwise position the value of $\partial v/\partial x$ is the same at all values of y in the range $85 \leqslant y^+ \leqslant 255$ (and zero elsewhere), and corresponds to that for $y^+ = 170$ (figure 15) at all y within the chosen range. The convection velocity of the velocity

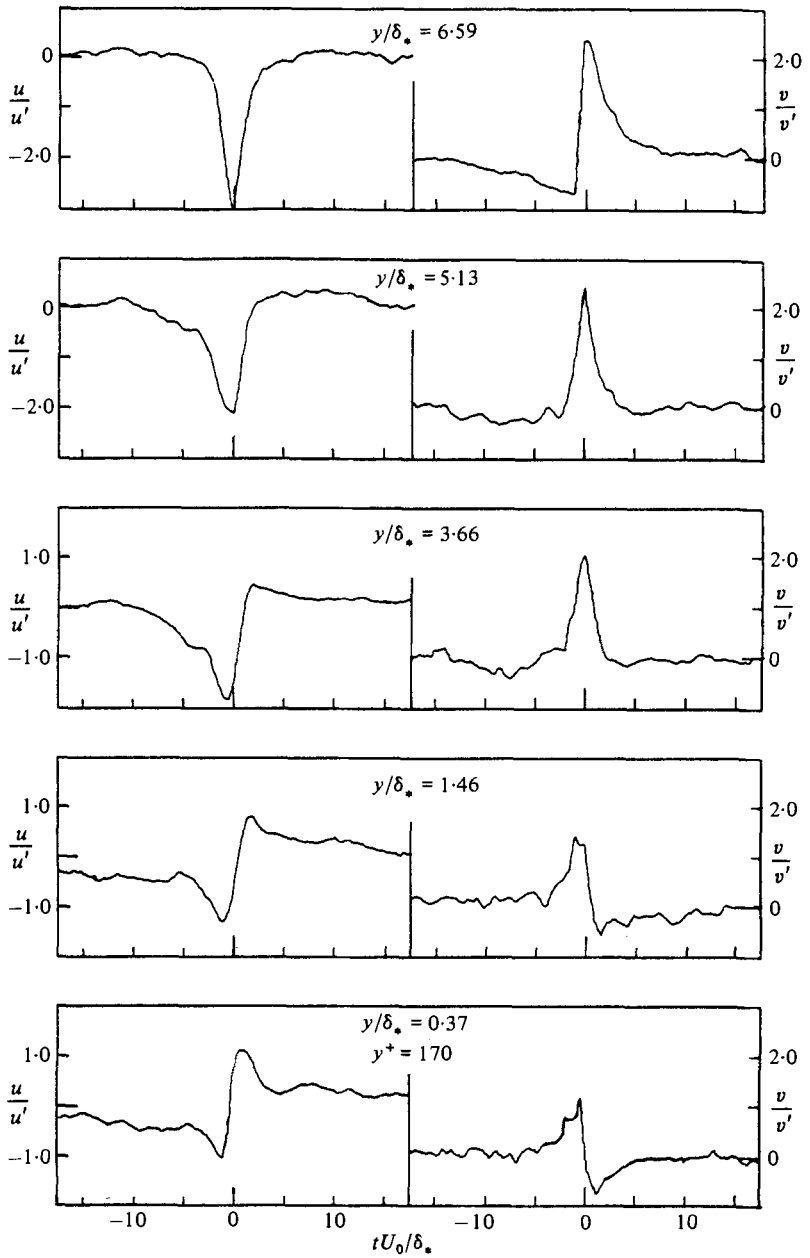

FIGURE 15. Ensemble-averaged time histories of conditionally sampled streamwise and normal components of velocity. Detection is based on the smoothed rectified high-frequency u-component at each y-value.

field has been taken as $U_c = 0{\cdot}64U_0$, the mean-flow velocity at $y^+ = 170$. The result presented in figure 16 is for $\partial v/\partial x$ having the values specified above over a very small distance in the spanwise (z) direction and zero at all other spanwise positions. Calculations have also been made with an exponential spanwise decrease in $\partial v/\partial x$ on either side of the plane of interest, and with extensions of the y^+ range; such modifications have an effect on the amplitude of the computed pressure pattern but not on its shape. The result certainly adds credibility to the pressure pattern proposed

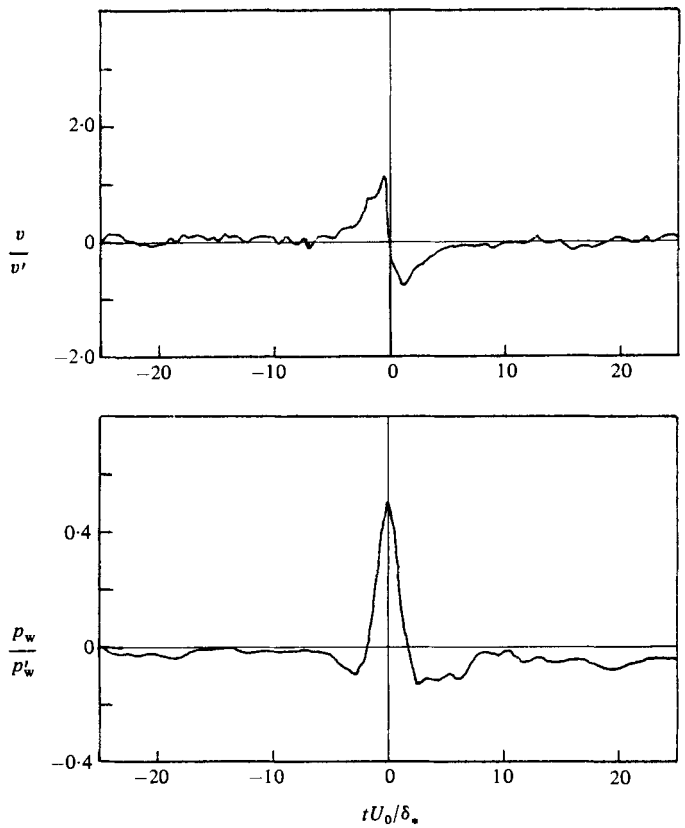

FIGURE 16. Calculated time history of wall pressure due to sources characterized by the indicated distribution of normal velocity component corresponding to $y^+ = 170$.

earlier (figure 14). Note that, because of the assumption that the velocity steps are simultaneously located on a line normal to the wall, the wall-pressure pattern predicted by this model must of necessity have a positive pressure peak occurring at exactly the same time as the maximum in $\partial v/\partial x$, that is, at the same time as the steps in the u- and v-components of velocity.

The model just considered is obviously a very simplified one. A more-realistic model should take account of the known properties of the flow near the wall, particularly the very small inclination to the wall of the turbulence structures associated with the velocity steps (as indicated by the measurements of Blackwelder & Kaplan (1976), Thomas (1977) and Kreplin & Eckelmann (1979)). Further, the pressure pattern that is obtained by conditioning on the velocity step at a given point in the boundary layer will, following (3), represent the integrated effect of all those pressure sources throughout the layer that are correlated with the velocity step structure at the given point. Two extreme cases may then be considered.

At one extreme, if the correlation of the velocity steps at different distances from the wall were to extend only over distances that are quite small in comparison with the thickness of the boundary layer, then, in a conditional-averaging process, the pressure pattern obtained would represent only that component of the pressure field due to the sources in the immediate vicinity of the velocity-measuring point. The contribution of the other uncorrelated sources would be zero, and the positive maximum of the pressure pattern would be essentially in phase with the maximum value of $\partial v/\partial x$, at the velocity measuring point, as in the model already considered.

At the other extreme, if the velocity steps at different distances from the wall were to be strongly correlated over all values of y, the pressure pattern would characterize the whole large-scale flow structure. In this case the same average pressure pattern would be obtained irrespective of the distance from the wall of the velocity measurement point. Furthermore, if the line of strongest correlation of the velocity steps were not normal to the wall, but inclined to it (as in the measurements of Blackwelder & Kaplan, Thomas and Kreplin & Eckelmann just referred to), there should be a time delay between detection based on some feature of the velocity step and the occurrence of the maximum of the wall pressure pattern; this time delay would vary with the y-coordinate of the detection point, and reflect the spatial configuration of the flow structure.

Close examination of the phasing between velocity and pressure time histories (figures 11*c*, *d*, 12, 13) shows that the maximum pressure does not occur at precisely the same time as the velocity step, indicating a situation somewhere between these two extremes. Existing correlation data can be used to elucidate this point further. For example, the correlations between the wall pressure and the v-component of velocity as measured by Willmarth & Wooldridge (1963) have a form that is consistent with the correlation between a velocity step and an associated pressure pattern of the type being considered here. A feature of them is that the time delay at which a given characteristic of the correlation (e.g. the zero-crossing) occurs depends only on the streamwise separation between pressure-transducer and hot-wire ξ and the local mean velocity U at the position of the velocity probe (varying linearly as ξ/U) irrespective of the distance of the velocity probe from the wall for $0{\cdot}1 \lesssim y/\delta_* \lesssim 3$ or $170 \lesssim y^+ \lesssim 5000$. These correlations therefore do not reflect the inclination of the flow structures to the wall. Whether or not this would also apply to conditions as close to the wall as $y^+ = 30$ is not clear, but it does suggest that the pressure source field further from the wall does not have a correlation extent that is very large in the y-direction. Unfortunately, such data are not available for distances as small as $y^+ = 30$, but the velocity-correlation data of Blackwelder & Kaplan (1976) and Kreplin & Eckelmann (1979) taken near the wall show that there is quite a strong correlation of the inclined velocity step structure over values of y^+ from zero to values in excess of 30. Therefore, on this evidence it seems likely that the conditionally sampled pressure pattern represents an overall pattern that is characteristic of this inclined structure near the wall.

To examine this possibility further, calculations, based upon (4), have been made to determine the pressure pattern that would be associated with such an inclined shear layer. The layer is assumed to be inclined to the wall along the geometrical trajectory given by Kreplin & Eckelmann (1979, figure 17) and it has further been assumed that the normal velocity has a linear rise over a streamwise distance of $2{\cdot}0\delta_*$ preceded and followed by a linear decrease at one-third of this rate. This distribution is shown in (our) figure 17 and has been chosen to resemble the scale of the measured distribution in figure 16. The magnitude of the velocity step has been taken to increase from zero at the wall and asymptotically approach a constant value as y increases; the mean velocity gradient has been taken as that given by Reichardt (1951). The results of the calculation are shown in figure 17. The main contributions to the calculated pressure come from sources in the region $0 \lesssim y/\delta_* \lesssim 1$, and it appears that essentially the same result would be obtained even if allowance were made for the change in character of the v-velocity step in the outer part of the boundary layer indicated by figure 15. The pressure maximum occurs at $x/\delta_* \approx 1{\cdot}0$ relative to the 'foot' of the

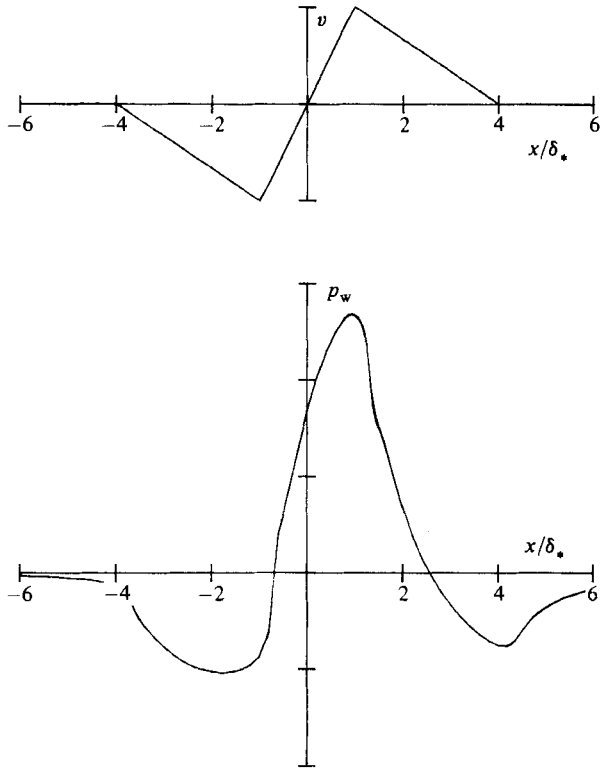

FIGURE 17. Calculated pressure pattern due to the inclined shear layer associated with large structure with the normal velocity distribution as shown.

shear layer, corresponding to a time difference of $tU_0/\delta_* \approx 1{\cdot}5$. This is a consequence of the inclination of the structure and broadly consistent with experimental observation (figure 13). It is noted also that because of the steep inclination of the structure near the wall the negative pressure loop ahead of the structure is somewhat reduced relative to the negative loop that follows behind.

Although the phase relation between the velocity and pressure will depend upon the nature of the scaling of both fluctuations with flow parameters, the calculations suggest that the ensemble-averaged pressure signals, conditioned upon the velocity, do indeed represent the pressure field associated with the inclined velocity step structure near the wall with negligible contribution from sources further from the wall.

Considering now Burton's result and the present data (figures 11*b–d*), in conjunction with a pressure signature of the velocity-step structure in the vicinity of the wall similar to that of figure 14, we see that they could be reconciled with each other if the detection time in the present experiments ((*c*) and (*d*)) were to correspond to a time after the first minimum and close to the first zero-crossing of the pressure pattern and that for (*b*) to the second minimum. In particular this could explain why the positive pressures in (*c*) and (*d*) are earlier than that for (*b*) by an amount $\Delta(tU_0/\delta_*) \approx 3$. A model that could explain how this difference might arise will now be considered. It should be emphasized, however, that, because we have only a little knowledge of the detailed shape and orientation of the velocity step structure and its dependence on wall and outer-layer variables, any such model has to be regarded as highly speculative.

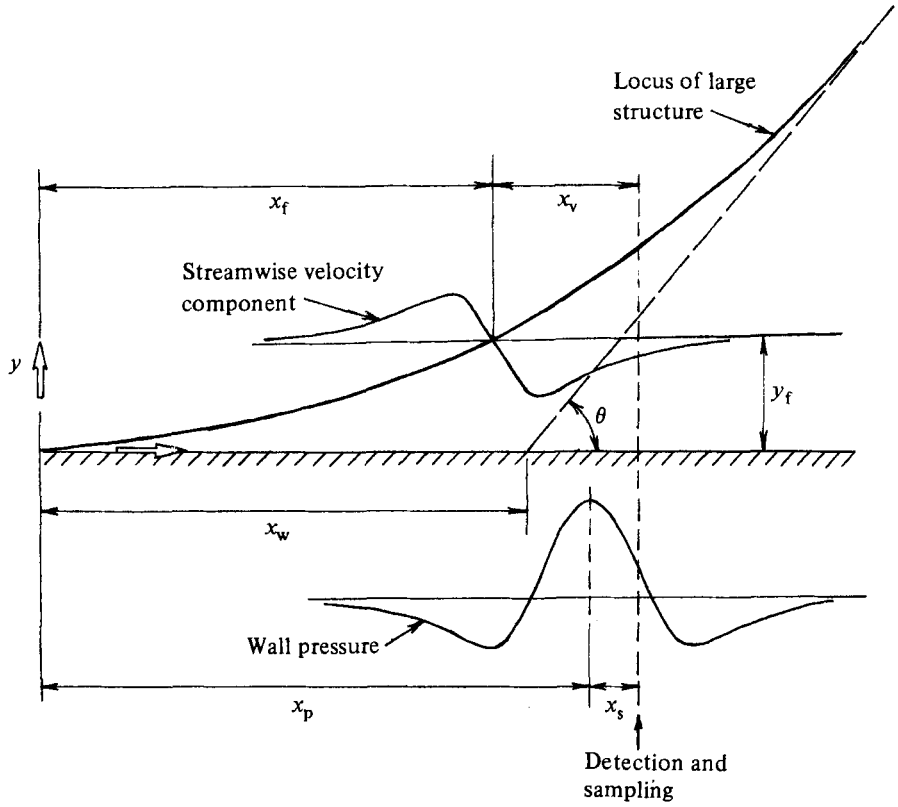

FIGURE 18. Diagrammatic representation of the velocity-step flow structure and its associated convected wall-pressure and velocity signatures.

We assume that the pressure pattern and flow structure have spatial relationships as indicated in figure 18, and that they have the following properties.

(i) The pressure pattern represents an overall signature of the portion of the large-scale flow structure associated with the velocity steps close to the wall.

(ii) The velocity and pressure patterns both scale with outer-layer variables even in the wall region.

(iii) The flow structure associated with the velocity step lies on a straight line inclined at an acute angle θ to the wall in the outer layer, but in the wall region, under the influence of mean-flow velocity gradients, becomes stretched out over large streamwise distances, to an extent determined by wall variables, taking up an 'average' shape such as that measured by Thomas (1977) and Kreplin & Eckelmann (1979).

Let the line through the zero-crossing points of the velocity steps be defined by the coordinates (x_f, y_f), and let detection be based on the velocity at a point at a distance x_v ahead of the zero-crossing point, at a particular value of y_f. In relation to the pressure pattern, detection will then occur at a distance x_s ahead of the pressure maximum given by

$$x_s = x_f + x_v - x_p,$$

where x_p is the distance downstream of the origin of the flow structure at which the pressure maximum occurs. If, in accordance with assumption (ii) above, $\overset{*}{x}_v$ (where $*$ indicates a length divided by δ_*) is regarded as a constant independent of the flow

Reynolds number $Re_\theta = U_0\theta/\nu$, and x_p^+ is assumed independent of Re_θ, it is appropriate to rewrite the preceding expression as

$$\overset{*}{x}_s = \overset{*}{x}_v - \frac{x_p^+ - x_f^+}{\delta_*^+}.$$

The measurements of Kreplin & Eckelmann (1979) of the detailed shape of the structure near the wall indicate $x_f^+ = 128$ and 215 at $y_f^+ = 15$ and 30 respectively. We now make a representative assignment $x_p^+ = 400$, and assume that, for the conditions leading to the results of the present experiments presented in figures 11 (*c*, *d*) (for which $y^+ = 30$ and $\delta_*^+ = 469$), sampling of the wall-pressure pattern has been centred on $\overset{*}{x}_s \sim 0{\cdot}9$. If allowance is made for the streamwise separation of the detector probe and the wall-pressure transducer ($0{\cdot}13\delta_*$) this implies that, for detector and pressure sensor at the same x, $\overset{*}{x}_v \approx 0{\cdot}9 + (400-215)/469 + 0{\cdot}1 \approx 1{\cdot}4$. Application of this value to the conditions of Burton's experiments ($y^+ = 15$ and $\delta_*^+ = 190$) leads to a corresponding value of $\overset{*}{x}_s$ of $1{\cdot}4 - (400-128)/190 \approx 0$. The difference in $\overset{*}{x}_s$ values of about 0·9 would imply sampling of the pressure pattern earlier in the present experiments by $\Delta(tU_0/\delta_*) \approx 1{\cdot}3$. (It might be noted that the assumption $x_p^+ = 400$, which seems a reasonable one, is somewhat at variance with the relative phasing of pressure and velocity indicated by figures 8 and 9. Those figures indicate that, in the spatial structure, the convection of which produces the observed temporal relationships, the pressure peak is located upstream of the zero-velocity point, and in fact in the region of the origin of the flow structure. This is physically unrealistic, and the observation should presumably be taken to indicate the order of experimental accuracy of the data.) Alternatively, it might be assumed that $\overset{*}{x}_w - \overset{*}{x}_p$ rather than x_p^+ is independent of Reynolds number, where x_w is the coordinate of the projection of the line of the flow structure in the outer region to the wall. In this case the expression for x_s can be written as

$$\overset{*}{x}_s = \overset{*}{x}_v + (\overset{*}{x}_w - \overset{*}{x}_p) - \frac{x_w^+ - x_f^+}{\delta_*^+}.$$

The assignment $x_w^+ = 700$ would be consistent with the general shape of the flow structure determined by Thomas (1977). Using this value and the same values of (x_f, y_f) as previously, we obtain $\overset{*}{x}_v + (\overset{*}{x}_w - \overset{*}{x}_p) \approx 0{\cdot}9 + (700-215)/469 + 0{\cdot}1 \approx 2{\cdot}0$ for sampling of the pressure pattern at $\overset{*}{x}_s \approx 0{\cdot}9$ in the present experiments. The corresponding value of $\overset{*}{x}_s$ for Burton's experiments is then

$$\overset{*}{x}_s \approx 2{\cdot}0 - (700-128)/190 \approx -1{\cdot}0.$$

The difference in $\overset{*}{x}_s$ values is now about 1·9, which would give a time difference of $\Delta(tU_0/\delta*) \approx 3$.

The model is based on obviously simplistic scaling assumptions and it takes no account of the continuous evolution and distortion of the flow structure which the convection velocity measurements by Kreplin & Eckelmann clearly show must be occurring. However, it does serve to indicate that the differences in conditionally sampled pressure patterns between the present experiments and those of Burton could result from the differences in Reynolds numbers. Similar considerations would explain the appearance of a negative pressure peak, close to the detection time, as the dominant feature of the pressure pattern obtained by Willmarth (1975), since the Reynolds number in Willmarth's experiment was very similar to that in Burton's. The absence from Willmarth's pattern of any local maxima or minima, apart from the minimum close to the time of detection, of course remains unexplained, although

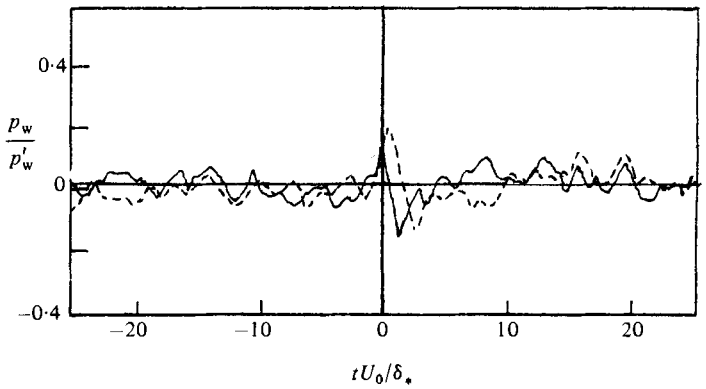

FIGURE 19. Ensemble-averaged time histories of the wall pressure at different Reynolds numbers. Detection is based on the smoothed rectified high-frequency component of the streamwise velocity component at $y^+ = 30$. ——, $Re_\theta = 4920$; --- $Re_\theta = 10200$.

the rather large size of transducer used ($d/\delta_* \approx 0{\cdot}4$, compared with $d/\delta_* \approx 0{\cdot}1$ in both Burton's and the present work) may be a contributing factor.

The notion that differences in pressure patterns are attributable to differences in Reynolds numbers is also supported by measurements made in the present investigation. Conditional sampling of the wall pressure on the basis of the smoothed rectified high-frequency component of the velocity signal at $y^+ = 30$, the procedure which led to figure 9 for $Re_\theta = 10200$, was also carried out in a flow with a lower Reynolds number $Re_\theta = 4920$. The pressure patterns for the two Reynolds numbers are compared in figure 19; they are consistent with sampling having taken place later at the lower Reynolds number (so that relative to the detection time a given feature of the pressure pattern appears earlier). With the reduction in Reynolds number there is a noticeable change from a pattern dominated by a positive pressure peak to one in which the positive peak has become less prominent and the following negative peak more so. The lower Reynolds number is much closer to (although still significantly higher than) that of Burton and Willmarth's experiments, and the pressure pattern corresponding to it shows a greater similarity to Burton's pattern. The time difference indicated by figure 19 is $\Delta(tU_0/\delta_*) \approx 1{\cdot}3$, which is roughly consistent with the Reynolds-number dependence indicated by the other experimental data.

7. Relation of characteristic patterns of wall pressure, wall shear and velocity variation to the ordered large-scale motion and to events in the burst–sweep cycle

7.1. *The characteristic wall-pressure pattern*

The considerations of §6 lead us to the conclusion that there is a characteristic wall-pressure pattern associated with the occurrence of sharp steps in the velocity components in the wall region and the intermittent high levels of small-scale velocity fluctuations that accompany them, and consequently with the burst–sweep cycle of events. The indications are that it is of the general form of figures 14 and 17, and, as we have seen, such a pattern could explain differences in ensemble-averaged pressure signals obtained by various sampling processes conditioned on the velocity fluctuations above and close to the wall. If this is the case, there remains the question of whether the ensemble-averaged pressure variation obtained from self-conditioned pressure sampling based on high levels of small-scale pressure fluctuations (figure 5)

and indicated by the correlation of figure 3 is a part of the same characteristic pattern, modified by statistical variations in combination with a sampling time which does not coincide with the maximum of the pressure pattern. It is possible that the answer to this question could have been provided by ensemble averages of pressure samples centred on new detection times on either side of the detection times that produced the patterns shown in figure 5, but such averages were not calculated because of the difficulty in setting a criterion to define these times. However, it is clear that patterns of the form of figure 5 could be produced by sampling a pressure pattern such as figure 14 at a time a little later than the point A in the latter, with degradation of the true pattern at times removed from the detection time (compare figure 12(*a*) and 13(*a*)). We are therefore inclined to the view that the self-conditioned pressure ensemble average of figure 5 is merely a variant of the characteristic wall-pressure signature of the velocity-step structure, which has the general form of figures 14 and 17. (We should remember of course that whether this conclusion is correct or not, the measured results show that the occurrence of high-frequency wall-pressure disturbances is intimately associated with a rapid fall in wall pressure.) Support for this view also comes from the fact that the convection velocity of the pattern yielded by self-conditioned pressure sampling is found to be $0{\cdot}67U_0$, precisely the same value as found by Burton (1974) for his pressure pattern derived from velocity conditioning. This then implies, as was concluded in §6.4, that the small-scale pressure fluctuations identified by high values of the smoothed rectified high-frequency pressure signal are also associated with the burst–sweep cycle.

Dinkelacker *et al.* (1977) have presented additional analysis of results obtained by Emmerling (1973) using their interferometry technique for obtaining instantaneous wall-pressure patterns. They identify several different types of pattern with different scales and convection velocities. In particular they discuss a pattern (their pattern A) that has a convection velocity of $0{\cdot}76U_0$ and an overall scale of the order of $0{\cdot}5\delta$. Dinkelacker *et al.* regard this pattern as being characterized (in time) by a region of overpressure followed by a region of underpressure. We suggest that these patterns could well be extended to include an additional negative loop, and identified with the characteristic pattern that we are now associating with the bursting process. The records of Dinkelacker *et al.* showing their pattern A are reproduced in figure 20. We have appended a scale of x/δ_* and have picked out with heavy lines pattern A plus our extensions to it. (It should be noted that, because of the low Reynolds number of the experiments, the patterns can be viewed as small-scale variations if considered in relation to wall variables, or as large-scale variations if considered in terms of outer-layer variables. We are taking the latter view.) The average distance between two minima over frames 37–66 is $3{\cdot}2\delta_*$. With $U_c = 0{\cdot}76U_0$ this corresponds to a time difference between the minima of $\Delta(tU_0/\delta_*) = 4{\cdot}2$. This is in remarkably good agreement with the corresponding value on the pattern of figure 14, which has been set only by consideration of the conditional-sampling results in §6.5. Additional spatial patterns that can be viewed in the same way are evident in Emmerling's data (his figure 16); but the correspondence must be treated with some caution since Emmerling, from consideration of a number of such spatial patterns of high-amplitude wall-pressure fluctuations (see his figure 18), was not able to discern a typical form of variation. Nevertheless, while recognizing the temptation to associate any portion of a fluctuating pressure record that shows successive negative, positive and negative regions with the pattern represented by figure 14, there are segments of Emmerling's samples that could well represent such patterns. Furthermore, Emmerling found convection velocities of the extrema of the characteristic spatial patterns (such as

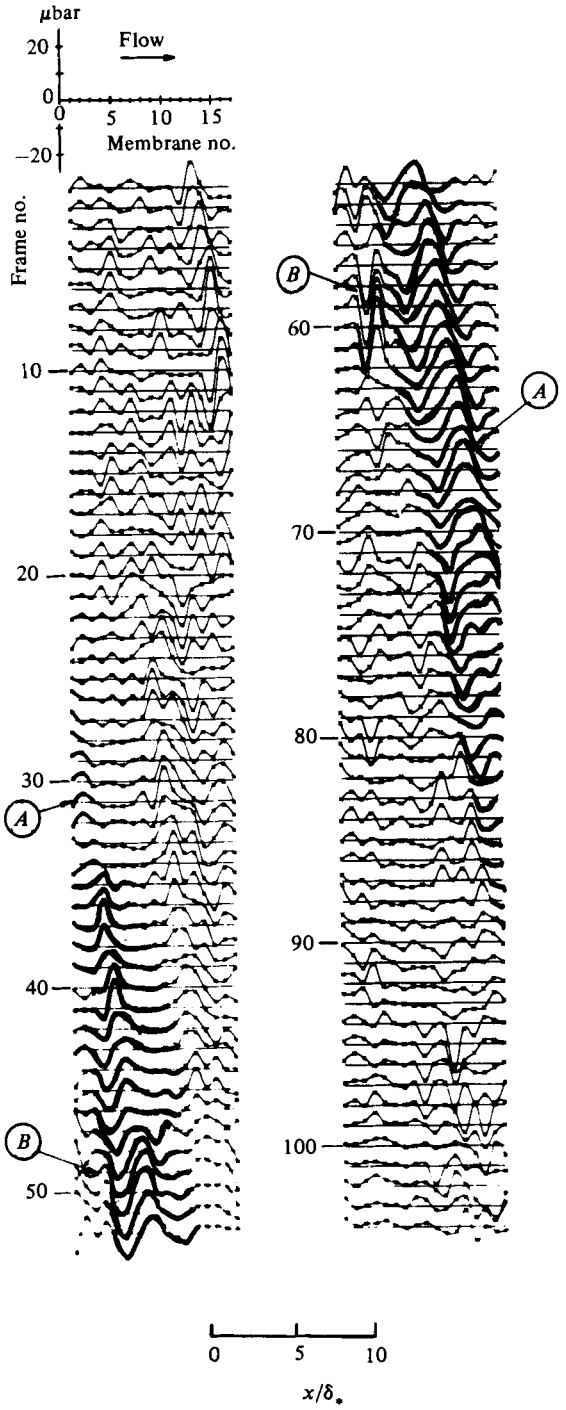

FIGURE 20. Instantaneous wall-pressure distributions in streamwise direction as determined by interferometry. Flow is from left to right, $U_0 = 8{\cdot}5$ m/s, time between consecutive maps is 0·14 ms. From Dinkelacker *et al.* (1977).

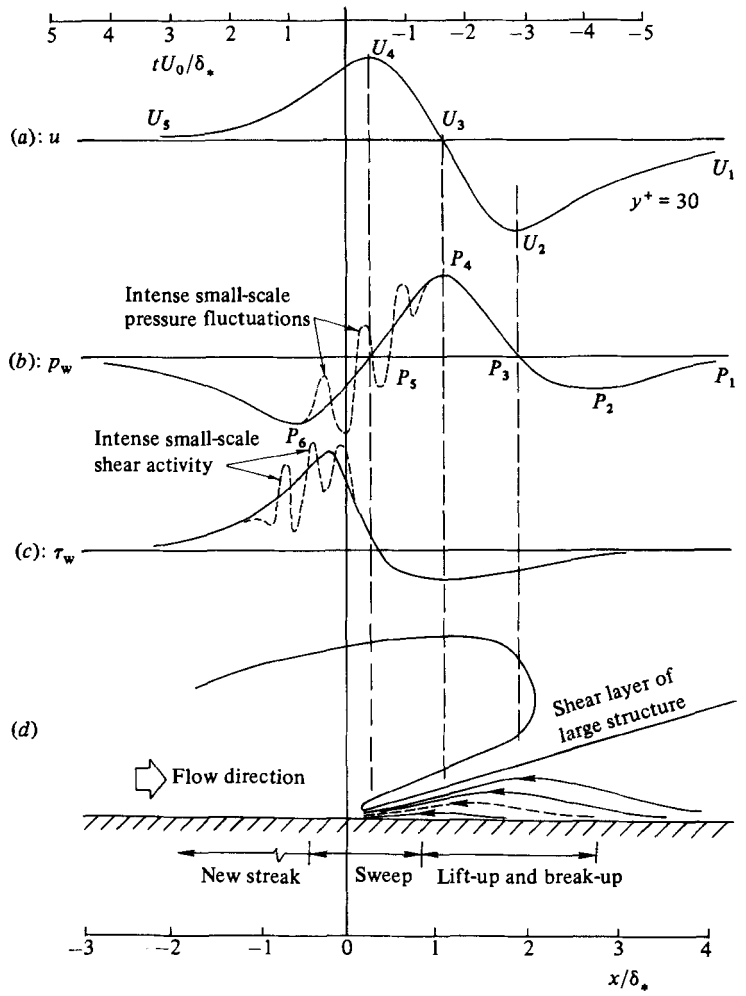

FIGURE 21. Distribution and phasing of (*a*) velocity, (*b*) wall pressure and (*c*) wall shear-stress fluctuations associated with the burst–sweep cycle. (*d*) Flow pattern near the wall in the region of the shear layer of the large structure. Locations of events in the burst–sweep cycle are shown.

pattern *A*) ranging from $0{\cdot}39U_0$ to $0{\cdot}82U_0$ but most commonly in the range $0{\cdot}53U_0$–$0{\cdot}73U_0$. The value of convection velocity of the pressure patterns obtained by self-conditioned sampling of the wall pressure in the present work, $0{\cdot}67U_0$, seems to be consistent with this. He also found the amplitude of fluctuation in these patterns to be of the order of $2p'_w$; ensemble averages with extrema generally in the range $0{\cdot}3$–$0{\cdot}8p'_w$ as measured here seem to be in keeping with this. Finally, in this section we note that Emmerling's value for the average period of occurrence of the patterns is $TU_0/\delta_* = 27$, which is very close to the burst rate determined by Rao *et al.* (1971), Lu & Willmarth (1973) and others.

7.2. *Time sequence of variation of wall pressure, wall shear and velocity*

Now, assuming, as indicated by the observations in §§4 and 5, that the high-amplitude high-frequency wall-pressure fluctuations and wall shear-stress fluctuations occur almost simultaneously, it is possible to establish the time sequence of variation of wall pressure, wall shear and streamwise velocity component which is associated with

the burst–sweep cycle; this is shown in figures 21(*a–c*). Spatial scales of the convected patterns that produce the time variation are also shown. All three patterns are convected at speeds of the order of $0{\cdot}67U_0$. Viewed from an observation point fixed in the boundary surface, the sequence is as follows. At some time before the arrival of the velocity step, u, p_w and τ_w are all negative and decreasing. The velocity then rises quite suddenly as a step, and it is this rise that triggers the high-frequency detection scheme. At the same time the pressure rises to a maximum (as implied by figures 8 and 9). Somewhat later the velocity at $y^+ = 30$ also reaches a maximum, at the time corresponding to that at which the pressure has fallen to zero; at this time the intense small-scale pressure activity is also occurring. The shear stress reaches a maximum at a slightly later time, at which point the pressure has become negative once more. Both small-scale shear-stress fluctuations and small-scale pressure fluctuations can be observed at this point. The approximate timescales of these events as determined from the experimental data are shown in the upper part of the figure.

7.3. *Structure of the ordered large-scale motion*

In another aspect of the present investigation, Thomas (1977) has made extensive measurements of correlations between the wall shear-stress fluctuations and velocity fluctuations throughout the layer, and between the low-frequency and high-frequency components of both the shear and the velocity. These lead to identification of the characteristics of the large-scale structure. The form arrived at for this structure (Thomas 1977; Brown & Thomas 1977) is similar in general character to that proposed by Laufer (1975) (although as will be seen later, there are significant differences in detail), and to that proposed by Falco (1977). It takes the form of a horseshoe vortex, which gives rise to the flow field in a plane normal to the wall through the centre of the vortex as shown in figure 22, where it is viewed, not in a laboratory reference frame, but in a reference frame moving with the structure itself. Additional support for this representation of the flow within the large structures is provided by the streamline pattern constructed from conditional averages of the u and v velocity components associated with it (Thomas 1977, 1979); this is shown in figure 23. The figure is based on conditional averages of u and v obtained using the high-frequency detection scheme (some of which, figure 15, have already been referred to) and an assumed large-structure convection speed of $U_c = 0{\cdot}8\,U_0$. (The form of the picture is, in fact, influenced very little by the precise value of convection speed that is chosen.) The arrows shown in the figure are velocity vectors whose length is given by $[(U(y)+\langle u\rangle - U_c)^2+\langle u\rangle^2]^{\frac{1}{2}}$ and whose angle is given by $\arctan[\langle v\rangle/(U(y)+\langle u\rangle - U_c)]$. It is further assumed that these ensemble-averaged velocity time histories can be positioned along a line inclined at 18° to the wall, the orientation found by Thomas (1977) to be representative of the large structure. The solid lines in the figure, although not strictly streamlines, serve as a visual guide to the form of the structure. The similarity between this experimentally determined figure and the structure shown schematically in figure 22 is apparent. Figure 22 also shows the likely form of the characteristic wall-pressure and shear-stress patterns which will be associated with a succession of the large structures.

A distinctive feature of the large structure is the shear layer on its back (upstream) surface, identified in the present work by the step in streamwise and normal components of velocity observed, by conditional sampling techniques, over the entire width of the boundary layer (figure 15 and Thomas 1977). This is in keeping with the results of Blackwelder & Kaplan (1976), who have made extensive measurements

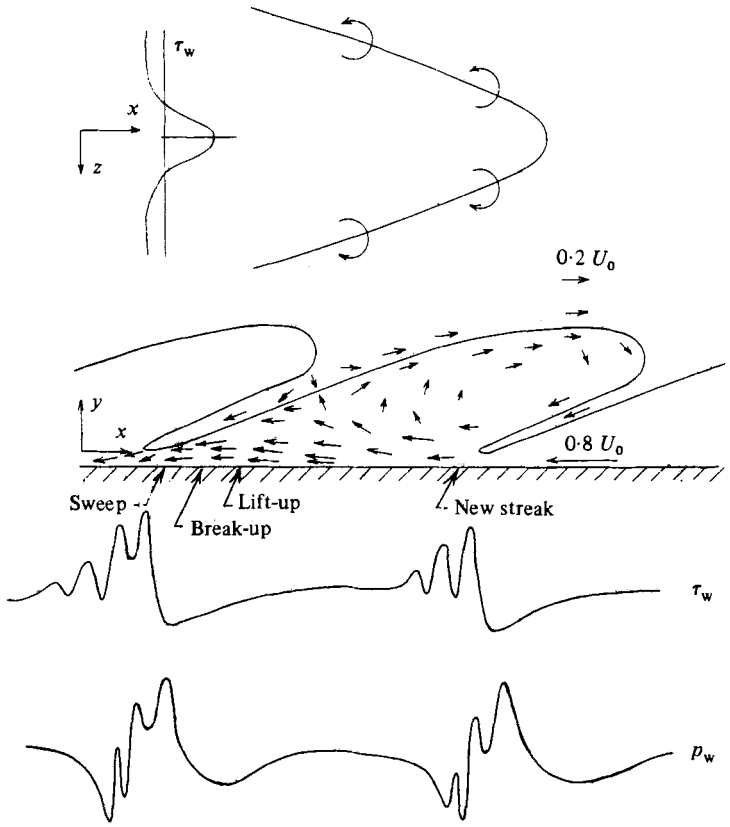

FIGURE 22. Large structure, associated pressure and shear distributions, and location of events in the burst–sweep cycle in a frame of reference moving with the large structure (following Brown & Thomas 1977).

of the streamwise velocity step throughout the wall region of the boundary layer using similar conditional-sampling techniques. The shear layer has also been identified by means of temperature steps in a slightly heated boundary layer (Chen & Blackwelder 1978) and by flow visualization (Falco 1977). The form of this layer in the vicinity of the wall has been investigated by Kreplin & Eckelmann (1979), whose data have been used in an earlier section. It will now be clear that the time origin chosen for figure 21 corresponds to the time at which the 'foot' of the shear layer in the immediate vicinity of the wall is above the observation point, as indicated in figure 21 (*d*).

7.4. *Phasing of characteristic pressure, shear and velocity variations with specific events in the burst–sweep cycle*

It is now possible to match the sequence of events in the burst–sweep cycle to the convected passage of the large structure over the observation point and the accompanying variations in wall pressure, wall shear and velocity. The fact that detection of the step in streamwise velocity at $y^+ = 30$ succeeds the occurrence of a burst, together with the deflection of the streamlines in the wall region relative to the large-scale structure away from and then towards the wall as the flow approaches the foot of the structure indicated by figure 23, allows the lift-up and break-up process to be located in the time-scale of figure 21. This results in the lift-up of a low-speed

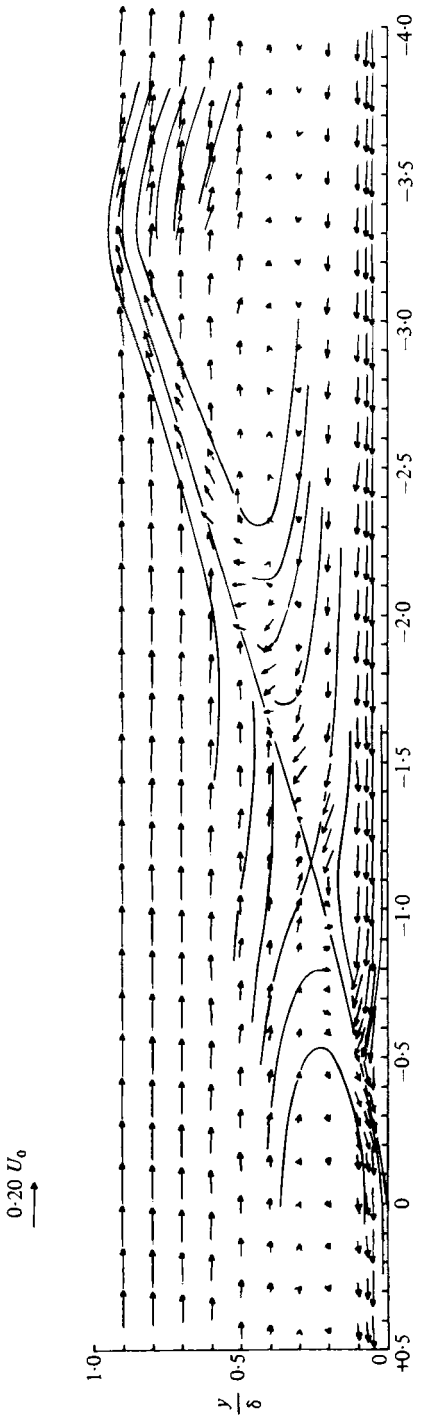

FIGURE 23. Experimentally determined streamline pattern of the large structure in a frame of reference moving with the structure. (Each vector represents an experimental determination of the conditionally sampled and averaged u- and v-components of velocity – see text.)

streak and its break-up becoming associated with the passage of the segment $P_2 P_3 P_4$ of the pressure pattern, so that the small-scale turbulence resulting from the break-up process would be seen at $y^+ = 30$ at the same time as the peak pressure P_4 reaches the observation point. Some of this small-scale turbulence would then be convected back towards the wall, towards the foot of the shear layer of the large-scale structure, as the sweep part of the cycle; as this happens it would give rise first to intense high-frequency pressure fluctuations and a little later, when it reaches the wall, to simultaneous high-frequency shear-stress fluctuations and high-frequency pressure fluctuations (as indicated by figures 21*b*, *c*). The turbulence generated by the burst would be swept under the foot of the large structure close to the wall, where the formation of new streaks, possibly by the process of combination of this fluid with fluid in a similar state from an adjacent burst, as suggested by Offen & Kline (1975), would be initiated. The locations of the various burst–sweep events in relation to the shear layer of the large structure are shown in figure 21 (*d*), and they can be seen to be consistent with the streamline patterns of figures 22 and 23 and the shear and pressure variations of figure 22. (It might be noted that because of the additional evidence available here the locations previously given by Brown & Thomas (1977) have been slightly modified.)

7.5. *Convection velocities of wall-pressure components*

Some comment on the convection velocity $0{\cdot}67U_0$ that we assign to the pressure pattern on the basis of the measurements presented in §6.3 should perhaps also be made, since it is considerably less than the value of about $0{\cdot}8U_0$ normally associated with large-scale motion in the boundary layer. In this connection, the following points should be considered.

(i) The resultant pressure pattern is dominated by the velocity step across the shear layer of the large structure in the wall region.

(ii) The pressure pattern is convected with the large structure, and the convection velocity of the large structure as might be expected, is lower in the inner than in the outer part of the layer (from velocity correlation measurements, Thomas (1977) finds convection velocities increasing from $0{\cdot}65U_0$ at $y = 0{\cdot}05\delta$ to $0{\cdot}80U_0$ at $y = 0{\cdot}75\delta$, indicating that the structure is slowly rotating, and a similar conclusion follows from the measurements of Kreplin & Eckelmann (1979)).

(iii) The value $0{\cdot}8U_0$ for the pressure field is measured only at quite large separation distances ($10\delta_*$ or even more – see Bull 1967), generally considerably greater than the separation distances (figure 6) on which figure 7 is based.

If these points are taken into account, the apparent inconsistency largely disappears. It would also be consistent with these considerations to associate the higher convection velocities of the wall-pressure field with large-scale motion in the outer part of the layer. This motion, which may or may not be part of the organized large structure that we have considered, is presumably responsible for the very large pressure patterns, having an extent of the order of the boundary-layer thickness in both the streamwise and transverse directions, which are observed by Dinkelacker *et al.* (1977) (their pattern *C*). These patterns have a scale considerably greater than the scale of the characteristic pattern that we have identified (and which we associate with pattern *A* of Dinkelacker *et al.*) and have convection velocities greater than $0{\cdot}8U_0$.

8. Role of convected pressure gradients associated with the characteristic wall-pressure pattern in the mechanism of the burst–sweep cycle

The patterns of variation of a number of fluctuating flow parameters – the velocity close to the wall, the wall pressure and the wall shear – and their phase relations in the vicinity of the foot of the shear layer on the back of the large-scale structure (as represented by figures 21 *a–c*) have been established, and these patterns have been shown to be intimately related to the burst–sweep cycle. However, even though we now have a consistent picture of the variation of velocity, pressure, and shear during the bursting process, we shall see that this does not lead to the identification of the associated causal relationships. In this section we wish to consider specifically the possible role of streamwise gradients of the wall pressure in the burst–sweep cycle.

We first recall that Laufer (1975), Offen & Kline (1975) and Willmarth (1975) have regarded the fluctuating pressure field as the dynamic link between ordered motion in the outer and inner regions of the boundary layer, and have attributed the lift-up of low-speed wall-region streaks, prior to bursting, to the imposition on them of adverse pressure gradients. Offen & Kline see the adverse pressure gradients as imposed on the low-speed streak by a wallward-moving sweep associated with a burst further upstream and giving rise to a local convected separation, while Willmarth considers that the adverse gradient originates from large-scale motion in the outer part of the layer.

In relation to these models the question arises as to whether pressure gradients associated with the characteristic pressure pattern that has been identified here, of the form of figure 14 or figure 17, applied to the flow in the wall region, could be responsible for initiating the lift-up of low-speed streaks and thereby the burst–sweep cycle of events, or whether it is merely a passive attendant of the large-scale structure. If adverse pressure gradients, that is, gradients for which $\partial p_w/\partial x > 0$, are indeed responsible for starting the burst–sweep cycle, then if the characteristic pressure pattern were to supply such gradients they would have to be those corresponding to the segment P_1P_2 or $P_4P_5P_6$ of figure 21 (*b*). Such causality would also imply that the adverse-pressure-gradient influence is a large-scale phenomenon rather than a small-scale one as envisaged by Offen & Kline. It is perhaps worth emphasizing that, as far as the downstream flow is concerned, a pressure gradient for which $\partial p_w/\partial x > 0$, irrespective of whether it is convected or stationary, constitutes an adverse gradient. It might be further noted that in the view from a frame of reference fixed in the wall the characteristic pressure pattern is convected downstream past the slow-moving fluid in the wall region. This relative motion results in the Lagrangian pressure variation Dp_w/Dt experienced by a fluid particle being of opposite sign to that of the convected spatial gradient $\partial p_w/\partial x$ that produces it; but it is fundamentally the spatial gradient $\partial p_w/\partial x$ itself that determines the magnitude and direction of the instantaneous force experienced by the fluid. Thus, considering the flow relative to the large structure, as in figure 21 (*d*), although it might be observed that the upstream flow of fluid near the wall towards the foot of the large structure is subjected to what is, to it, an essentially stationary adverse pressure gradient $P_2P_3P_4$, this gradient does not (even though its negative $\partial p_w/\partial x$ would subject any fluid particle to a positive Dp_w/Dt) represent an adverse pressure gradient in the sense required to produce streak lift-up. It is true that this flow when viewed from the large structure has diverging streamlines and is decelerated in the upstream direction as it negotiates the pressure rise $P_2P_3P_4$, but when viewed from a fixed observation point in the wall these same streamlines become transformed to convergent ones and the (unchanged)

upstream deceleration is more appropriately seen as a downstream *acceleration* relative to the wall.

The phasing relations that have been determined (figure 21) therefore indicate that the initiation of the lift-up process occurs at a time when the fluid involved is subjected by the convected characteristic pressure pattern to a *favourable* pressure gradient; they indicate that the adverse-pressure-gradient segments of the patterns are not the cause of lift-up of the low-speed streaks.

On the other hand, we should not overlook the fact that there is an inherent uncertainty in the experimental statistical averages on which the phasings assigned in figure 21 are based. It seems improbable, although not inconceivable, that this could be large enough to have produced the phasing shown in figure 21 when in reality the initiation of lift-up coincides with the passage of the adverse gradient segment P_4P_5 of the characteristic pressure pattern. If the latter were to be the case, an essential feature of the adverse-pressure-gradient models would be realized. We should then have to ask whether the magnitude, duration of application (residence time), and possibly other properties also, of the P_4P_5 gradient are sufficient to cause lift-up of the low-speed streaks. This is not an easy question to answer. However, we might expect to get some indication of the ability of the P_4P_5 adverse pressure gradient to cause lift-up by comparing it with the inertia of the fluid in the wall region to which it would have to be applied. In this event the timing of the pressure pattern in figure 21 would have to be changed to bring the $P_4P_5P_6$ pressure gradient into phase with the $U_2U_3U_4$ velocity gradient, and it is the effect of these two gradients that have to be compared. The appropriate inertia term for comparison with the pressure gradient is $\rho(\partial U/\partial t + U\,\partial U/\partial x)$, or, since the effect of convection of the flow patterns is to make $\partial/\partial t = -U_c\,\partial/\partial x$, $-\rho(U_c - U)(\partial U/\partial x)$, a result that could also be obtained by considering only the convective acceleration in a frame of reference moving with the large structures, with respect to which the flow in the wall region is quasi-steady (as in figure 21*d*). We take the view that, because the residence time of the pressure gradient is short (compared with, say, the duration of application of pressure gradients that produce significant effects on the overall streamwise development of a turbulent boundary layer), the relevant value of this inertia term is that at a distance y_s from the wall that is typical of the scale of the low-speed streaks in a direction normal to the wall (and not that at the wall itself, where of course the inertia term becomes zero). An evaluation of the ratio

$$\frac{\text{inertia force}}{\text{pressure force}} = \frac{\left[\rho(U_c - U)\dfrac{\partial U}{\partial x}\right]_{y=y_s}}{\dfrac{\partial p_w}{\partial x}}$$

is therefore required. Furthermore, if we consider the value of this ratio at wall distances in the range $3 \leqslant y^+ \leqslant 30$, then $y = y_s$ will be adequately included (see for example the summary of wall-streak scales given by Cantwell 1981).

If the amplitude and scale of the pressure pattern are taken as $A_p p'_w$ and L_p respectively, where A_p is a proportionality constant, then $\partial p_w/\partial x$ may be estimated as $A_p p'_w/L_p$. Similarly, with the amplitude and scale of the corresponding velocity pattern taken as $A_u u'$ and L_u, $\partial U/\partial x$ may be estimated as $A_u u'/L_u$. Then with $U^+ = U/U_\tau$, the required ratio becomes

$$\frac{A_u}{A_p}\frac{L_p}{L_u}\frac{u'}{U_\tau}(U_c^+ - U^+)\Big/\frac{p'_w}{\tau_w}.$$

Self-consistent values of A_u, A_p, L_u and L_p can be estimated from the results of the present work. Thus the velocity variation associated with the velocity-pattern segment $U_2 U_3 U_4$ is equivalent to a change of about $2u'$ over a lengthscale of about $1{\cdot}5\delta_*$ (values which are also in agreement with those of Blackwelder & Kaplan 1976), in which case $A_u = 2$ and $L_u = 1{\cdot}5\delta_*$; and the pressure variation associated with the pressure-pattern segment $P_4 P_5 P_6$ is equivalent to $0{\cdot}3$–$0{\cdot}8 p'_w$ over a lengthscale of $1{\cdot}5\delta_*$, so that $A_p \leqslant 0{\cdot}8$ and $L_p = 1{\cdot}5\delta_*$. With the additional assignments $p'_w/\tau_w \approx 3$, $U_0^+ \approx 30$, $U_c = 0{\cdot}67 U_0$, and $U_c^+ \approx 20$, these values lead to

$$\frac{\text{inertia force}}{\text{pressure force}} \geqslant \frac{5}{6}\frac{u'}{U_\tau}(20 - U^+).$$

With typical established values for u'/U_τ and U^+ the following numerical values are obtained:

$y^+ =$	3	5	7·5	10	20	30,
$u'/U_\tau =$	1·0	1·6	2·3	2·5	2·7	2·5,
$U^+ =$	3·0	5·0	7·5	9·4	12·2	13·5,
$\dfrac{\text{inertia force}}{\text{pressure force}} \geqslant$	14·2	20·0	24·0	22·1	17·6	13·5.

They show that the ratio of inertia force to pressure force has a maximum value in the region of $y^+ = 7{\cdot}5$ and that over the whole range of y^+ under consideration the inertia forces are at least an order of magnitude larger than the pressure forces. They therefore indicate that even if the phasing shown in figure 21 were to be in error to such an extent as to allow the passage of the segment $P_4 P_5 P_6$ of the characteristic pressure pattern to coincide in time with the onset of lift-up of a low-speed streak, the adverse pressure gradient associated with the characteristic wall-pressure pattern would not be of sufficient strength to initiate the lift-up.

The considerations of this section therefore strongly suggest that streamwise pressure gradients associated with the convected wall-pressure pattern characteristic of the large organized flow structures do not play an essential part in initiating the lift-up of low-speed streaks and hence the burst–sweep sequence.

It may also be pertinent to point out that the present discussion has of necessity been confined to the effects of *streamwise* pressure gradients. In view of the conclusion reached here, it may well be that serious consideration is needed of the role of the pressure gradient $\partial p/\partial y$ normal to the wall, significant values of which, generated perhaps by rotation of the large flow structures, may instead provide the link between the small-scale and large-scale organized motions.

9. Conclusion

The experimental results and calculations that have been presented provide strong evidence that the burst–sweep sequence of events in the wall region of a turbulent boundary layer is closely associated with a characteristic and identifiable variation in the wall pressure that accompanies the convected passage of a large organized flow structure whose scale is of the order of the boundary-layer thickness. The dominant feature of the large structure, as shown by several previous investigations, is a shear layer which forms its upstream surface, and which, except in the immediate vicinity of the wall, is inclined to the wall at an angle of about 18°; this feature has also been identified in the present work by the step in conditionally averaged streamwise and normal velocity components over the entire width of the boundary layer. This shear layer appears to be responsible also for the characteristic variations of wall shear and

velocity close to the wall, which by means of correlation and conditional sampling techniques have also been identified and shown to be intimately associated with the burst–sweep cycle.

It is deduced from the results presented that the characteristic spatial pattern of wall pressure associated with the burst–sweep cycle consists of a region of positive pressure with an extent of about $1{\cdot}5$–$2{\cdot}0\delta_*$, with a region of negative pressure having a pressure minimum to either side of it, the distance between pressure minima being about $3{\cdot}0$–$3{\cdot}5\delta_*$. The pattern is convected at a speed of $0{\cdot}67U_0$. There is a significant resemblance between this pattern and features of the instantaneous surface-pressure patterns obtained by Emmerling (1973) and Dinkelacker *et al.* (1977) using an interferometry technique. Calculation of the pressure pattern that would accompany the shear layer on the upstream surface of the large structures leads to a pattern of closely similar form to that inferred from the experimental data.

The phase relations between the pressure and velocity and wall shear stress during the bursting process have been established. They indicate that at the onset of the burst–sweep sequence the fluid in the wall region which is involved is subjected to a favourable, not an adverse, pressure gradient as a result of convection of the characteristic wall-pressure pattern, and hence that the pressure pattern is not responsible for initiating the process.

The order of magnitude of the adverse pressure gradients of the characteristic wall-pressure pattern in relation to the inertia of the associated flow in the wall region has also been considered; this comparison suggests that, even if the phasing were appropriate, these adverse pressure gradients would not be of sufficient strength to trigger the burst–sweep process, and in this sense reinforces the conclusion reached on the basis of the experimentally measured phase relations. The conclusion is therefore that the characteristic pressure pattern associated with the large organized flow structures is not the direct cause of the bursting process.

The authors wish to express their appreciation to Mr D. Morrison, Mr H. Bode, Mr P. Walker and Mr G. Osborne of the Department of Mechanical Engineering, University of Adelaide, for their technical assistance. Financial assistance provided by the Australian Research Grants Committee at various times during the course of the project (1974–1977) is gratefully acknowledged. Thanks are also due to Dr A. Dinkelacker of the Max-Planck-Institut für Strömungsforschung, Göttingen, Federal Republic of Germany, for permission to reproduce figure 20.

REFERENCES

Antonia, R. A. 1972 *J. Fluid Mech.* **56**, 1.

Blackwelder, R. 1977 *Phys. Fluids Suppl.* **20**, S232.

Blackwelder, R. F. & Haratonidis, J. H. 1980 *Bull. Am. Phys. Soc.* **25**, 1094.

Blackwelder, R. F. & Kaplan, R. E. 1976 *J. Fluid Mech.* **76**, 89.

Brown, G. L. & Davey, R. F. 1971 *Rev. Sci. Instrum. Notes* **42**, 1729.

Brown, G. L. & Thomas, A. S. W. 1977 *Phys. Fluids Suppl.* **20**, S243.

Bull, M. K. 1967 *J. Fluid Mech.* **28**, 719.

Bull, M. K. & Lim, K. B. 1968 In *Proc. 3rd Australasian Hydraul. and Fluid Mech. Conf.*, p. 143.

Bull, M. K. & Thomas, A. S. W. 1976 *Phys. Fluids* **19**, 597.

Burton, T. E. 1974 *M.I.T. Acoustics and Vibration Lab. Rep.* no. 70208–10.

Cantwell, B. J. 1981 *Ann. Rev. Fluid Mech.* **13**, 457.

Chen, E. P. & Blackwelder, R. F. 1978 *J. Fluid Mech.* **89**, 1.

Corino, E. R. & Brodkey, R. S. 1969 *J. Fluid Mech.* **37**, 1.

DINCKELACKER, A., HESSEL, M., MEIER, G. E. A. & SCHEWE, G. 1977 *Phys. Fluids Suppl.* **20**, S216.

EMMERLING, R. 1973 *Max-Planck-Institut für Strömungsforschung, Bericht* no. 9.

FALCO, R. E. 1977 *Phys. Fluids Suppl.* **20**, S124.

KAPLAN, R. E. & LAUFER, J. 1969 In *Proc. 12th Int. Congr. Appl. Mech.*, p. 236.

KIM, H. T., KLINE, S. J. & REYNOLDS, W. C. 1971 *J. Fluid Mech.* **50**, 133.

KLINE, S. J., REYNOLDS, W. C., SCHRAUB, F. A. & RUNDSTADTLER, P. W. 1967 *J. Fluid Mech.* **30**, 741.

KREPLIN, H. P. & ECKELMANN, H. 1979 *J. Fluid Mech.* **95**, 305.

KOVASZNAY, L. S. G., KIBENS, V. & BLACKWELDER, R. F. 1970 *J. Fluid Mech.* **41**, 283.

KRAICHNAN, R. H. 1956 *J. Acoust. Soc. Am.* **28**, 378.

LAUFER, J. 1972 *1st Naz. Alta. Mat. Symp. Math.* **9**, 299.

LAUFER, J. 1975 *Ann. Rev. Fluid Mech.* **7**, 307.

LAUFER, J. & BADRI NARAYANAN, M. A. 1971 *Phys. Fluids* **14**, 282.

LILLEY, G. M. & HODGSON, T. H. 1960 *AGARD Rep.* no. 276.

LIM, K. B. 1971 Ph.D. thesis, Dept Mech. Engng, University of Adelaide.

LU, S. S. & WILLMARTH, W. W. 1973 *J. Fluid Mech.* **60**, 481.

MOLLO-CHRISTENSEN, E. 1971 *A.I.A.A. J.* **9**, 1217.

NYCHAS, S. G., HERSHEY, H. C. & BRODKEY, R. S. 1973 *J. Fluid Mech.* **61**, 513.

OFFEN, G. R. & KLINE, S. J. 1974 *J. Fluid Mech.* **62**, 223.

OFFEN, G. R. & KLINE, S. J. 1975 *J. Fluid Mech.* **70**, 209.

RAO, K. N., NARASIMHA, R. & BADRI NARAYANAN, M. A. 1971 *J. Fluid Mech.* **48**, 339.

REICHARDT, H. 1951 *Z. angew. Math. Phys.* **31**, 208.

THOMAS, A. S. W. 1977 Ph.D. thesis, Dept Mech. Engng, University of Adelaide.

THOMAS, A. S. W. 1979 *AGARD*-CPP-271, *Turbulent Boundary Layers – Experiments, Theory and Modeling.*

THOMAS, A. S. W. & BROWN, G. L. 1977 In *Proc. 6th Australasian Hydraul. and Fluid Mech. Conf.*, p. 407.

WILLMARTH, W. W. 1975 *Adv. Appl. Mech.* **15**, 159.

WILLMARTH, W. W. & WOOLDRIDGE, C. E. 1962 *J. Fluid Mech.* **14**, 187.

WILLMARTH, W. W. & WOOLDRIDGE, C. E. 1963 *AGARD Rep.* no. 456.